Supporting Information

Regioselective Green Electrochemical Approach to the Synthesis of Nitroacetaminophen Derivatives

Eslam Salahifar, Davood Nematollahi*, Mehdi Bayat, Amir Mahyari and Hadi Amiri Rudbari

Faculty of Chemistry, Bu-Ali Sina University, Hamedan, Iran, Zip Code: 65178-38683. E-mail: **nemat@basu.ac.ir**, Fax:+98-813-8257407

Table of contents

1. Experimental section ……...page 4

2. Controlled-potential synthesis ……. page 5

3. Constant current electrolysis……page 7

4. FTIR spectrum of **2NPAC**.....page 12

5. Mass spectrum of **2NPAC** .....page 13

6. ^{1}H NMR spectrum of **2NPAC** .....page 14

7. Expanded ^{1}H NMR spectrum of **2NPAC** .....page 15

8. ^{13}C NMR spectrum of **2NPAC** page 16

9. Expanded ^{13}C NMR spectrum of **2NPAC** page 17

10. Thin layer chromatography of **2NPAC**(electrochemical synthesis) .....page 16

11. Thin layer chromatography of **2NPAC**(chemical synthesis) .....page 19

12. FT-IR spectra of **2NPAC** and **3NPAC** obtained from chemical synthesis ....page 20

13. Mass spectrum of **3NPAC**(chemical synthesis).....page 21

14. FT-IR spectra of **2NPAC** (electrochemical &chemical methods) .....page 22

15. UV-Vis spectra of **2NPAC** & **3NPAC**.....page 23

16. FT-IR spectrum of **2NOAC**.....page 24

17. Mass spectrum of **2NOAC** .....page 25

18. ^{1}H NMR spectrum of **2NOAC** .....page 26

19. Expanded ^{1}H NMR spectrum of **2NOAC**.....page 27

20. ^{1}H NMR spectrum of **2NOAC** (with D_2O) .....page 28

21. Expanded ^{1}H NMR spectrum of **2NOAC** (with D_2O).....page 29

22. ^{13}C NMR spectrum of **2NOAC** .....page 30

23. ORTEP view of X-ray crystal structure of **2NPAC** ……page 31

24. FTIR spectrum of **2NAPIP** ….. ……page 32

25. Mass spectrum of **2NAPIP** ……...page 33

26. ^{1}H NMR spectrum of **2NAPIP** ..... page 34
27. Expanded ^{1}H NMR spectrum of **2NAPIP** ..... page 35
28. Expanded ^{1}H NMR spectrum of **2NAPIP** ..... page 36
29. ^{13}C NMR spectrum of **2NAPIP** ..... page 37
30. Expanded ^{13}C NMR spectrum of **2NAPIP** ..... page 38
31. Cyclic voltammograms of **APIP** and **2NAPIP** ..... page 39
32. Calculated natural charge for **PBQ and OBQ** ……..……..…….page 40
33. The chemical structures of the possible nitrated compounds ……..….page 41
34. Calculated LUMO for **2NPAC**, **3NPAC**, **2NOAC** and **5NOAC**……. page 42
35. LUMO coefficient of **PBQ**,**OBQ** and **APIP$_{ox}$**…….……..page 44
36. Electrochemical oxidation of **NHPA**…….……page 46

Experimental section

General remarks

The working electrode used in the cyclic voltammetry experiments was a glassy carbon disc (1.8 mm diameter) and a glass carbon rod was used as the counter electrode. The working electrode used in macro-scale electrolysis and controlled-potential coulometry was an assembly of four ordinary soft carbon rods (6 mm diameter and 4 cm length), placed as single rods in the edges of a square with a distance of 3 cm, and a large stainless steel cylinder (25 cm^2 area) constituted the counter electrode. The electrochemical nitration were performed under controlled-potential condition in a two compartments cell, separated by an ordinary porous fritted-glass diaphragm (a tube with 1.5 cm diameter) and equipped with a magnetic stirrer. Acetaminophen (**PAC**), *N*-(2-hydroxyphenyl)acetamide (**OAC**), 1-(4-(4-hydroxyphenyl)piperazin-1-yl)ethanone (**APIP**), acetic acid and sodium acetate were obtained from commercial sources. These chemicals were used without further purification. The glassy carbon electrode was polished using alumina slurry (from Iran Alumina Co.). More details are described in our previous paper.[26]

Computational details

The geometries of all species in the gas phase were fully optimized at BP86/Def2-TZVPP level of theory using Gaussian 03.18.Vibrational frequency analysis, calculated at the same level of theory, indicates that optimized structures are at the stationary points corresponding to local minima without any imaginary frequency. Also NBO analyzes19 were carried out at the mentioned levels of theory. A starting molecular-mechanics structure for the ab initio calculations was obtained using the HyperChem 5.02 program.

Controlled-potential synthesis of 2NPAC, 2NOAC and 2NAPIP

A solution of acetate buffer solution (pH = 5.0, *c* = 0.2 M), containing **PAC** (or **OAC** or **APIP**), (0.25 mmol), was electrolyzed in a divided cell at 0.45 (in the case of **PAC**) and 0.55 (in the case of **OAC**) V and 0.30 vs. Ag/AgCl (3M) (in the case of **APIP**) in the presence of nitrite ion (1 mmol). The electrolysis was terminated when the decay of current became more than 95%. At the end of electrolysis, the aqueous layer was extracted three times with ethyl acetate (90 mL). The combined organic extracts were dried with $MgSO_4$ and evaporated in vacuum. **2NPAC**, **2NOAC** and **2NAPIP** were obtained after recrystallization in a mixture of chloroform/diethylether (40/60, v/v). They were characterized by IR, ^{1}H NMR, ^{13}C NMR, MS and SCXRD.

N-(4-hydroxy-3-nitrophenyl)acetamide ($C_8H_8N_2O_4$) (2NPAC)

Isolated yield: 85%. Mp=158-160 ^{o}C. IR (KBr): 3433, 3287, 3189, 2960, 2926, 2855, 1661, 1542, 1482, 1341, 1271, 1099, 1019, 813, 755, 629, 554, 513 cm^{-1}. ^{1}H NMR (400 MHz, DMSO-d_6): δ 2.03 (s, 3H, methyl), 7.09 (d, 1H, *J* = 8.8 Hz), 7.61 (dd, 1H, *J* = 9.0, *J* =2.8 Hz), 8.30 (d, 1H, *J* =2.8 Hz), 10.09 (s, 1H), 10.7 (broad, ~1H). ^{13}C NMR (125 MHz, D_2O): δ 23.6, 114.6, 119.4, 126.8, 131.1, 135.5, 148.1, 168.2. MS (EI) m/z (relative intensity): 196 (71), 154 (100), 137 (14), 109 (57), 80 (28), 52 (34).

N-(2-hydroxy-3-nitrophenyl)acetamide ($C_8H_8N_2O_4$) (2NOAC)

Isolated yield: 68 %. Mp = 228-230 ^{o}C. IR (KBr): 3313, 3095, 2924, 2853, 1668, 1608, 1532, 1447, 1337, 1269, 1215, 1174, 1080, 990, 852, 730, 603, 524 cm^{-1}. ^{1}H NMR (400 MHz, DMSO-d_6): δ 2.08 (s, 3H, methyl), 3.40 (s, 1H, NH, disappeared by the addition of D_2O), 6.03 (t, 1H, *J* =8.1 Hz), 7.42 (dd, 1H, *J* =9.0 and *J* =1.6 Hz), 8.05 (dd, 1H, *J* = 7.6 and *J* =1.6 Hz), 9.14 (s, ~1H, OH, disappeared by the

addition of D_2O). ^{13}C NMR (100 MHz, DMSO-d_6): δ 24.6, 108.5, 119.9, 120.1, 134.3, 134.9, 159.9, 168.6. MS (EI) m/z (relative intensity): 196 (50), 154 (100), 137 (25), 109 (75), 80 (25), 52(19).

1-(4-(4-hydroxy-3-nitrophenyl)piperazin-1-yl)ethanone ($C_{12}H_{15}N_2O_4$) (2NAPIP)

Isolated yield: 78 %. Mp = 118-119 ^oC. IR (KBr): 3519, 3449, 2973, 2853, 1614, 1531, 1446, 1425, 1246, 1171, 960, 757, 596 cm^{-1}. ^1H NMR (600 MHz, $CDCl_3$): δ 2.15 (s, 3H, methyl), 3.10 (tt, 4H, piperazine, *J* = 4.8 Hz), 3.64 (t, 2H, *J* = 4.8 Hz), 3.78 (t, 2H, *J* = 4.8 Hz), 7.10 (d, 1H, *J* = 9.6 Hz), 7.31 (dd, 1H *J* =3Hz), 7.50 (d, 1H, *J* = 3.0 Hz), 10.30 (s, 1H, OH). ^{13}C NMR (200 MHz, $CDCl_3$): δ 21.4, 41.2, 46.0, 50.1, 50.2, 110.5, 120.7, 129.1, 133.3, 144.6, 150.0, 169.1. MS (EI) m/z (relative intensity): 265 (90), 250 (9), 222 (18), 193 (100), 180 (27), 56(36).

Constant current synthesis of 2NPAC, 2NOAC and 2NAPIP

To increase the feasibility of the method, the synthesis of **2NPAC**, **2NOAC and 2NAPIP** was also performed via the constant current electrolysis in the same conditions as described for controlled-potential electrolysis. To achieve high product yield, the effect of current density was investigated in the range 0.01 to 2.5 mA/cm^2, in acetate buffer solution (pH = 5.0, *c* = 0.2 M), containing **PAC** (**OAC** or **APIP**) and nitrite ion when the charge consumed in the redox process was 50 C.

Fig. S1 shows the effect of current density on the generated potential during constant-current synthesis of **2NPAC**.

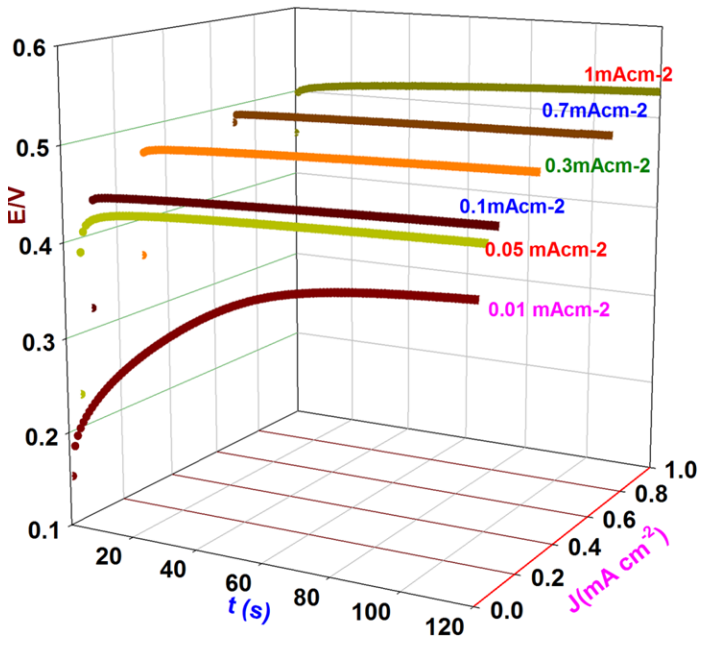

Fig. S1. The potential-time diagram during constant current electrolysis of **PAC** (0.25 mmol) in the presence of nitrite ion (1 mmol), at glassy carbon electrode in acetate buffer solution (pH = 5.0, *c* = 0.2 M). Rotation rate: 1000 rpm. Temperature = 25±1 °C.

This Fig. shows that when the applied current is 0.1 mA/cm^2, the cell potential is about 0.45 V vs. Ag/AgCl (3M), which is about half wave potential of **PAC**/**PBQ** redox couple, and is the

appropriate potential for the synthesis of **2NPAC**. Therefore current density, 0.1 mA/cm^2 was selected as an optimum current density. Our data show that, the highest product yield (84%) was obtained at current density of 0.1 mA/cm.

The current efficiency for various current densities during the synthesis of **2NPAC** is shown in Fig. S2. The current density varied from 0.1 to 1.0 mA/cm^2, while the other parameters are kept constant. The effect of current density on the current efficiency is shown in Fig. S2.

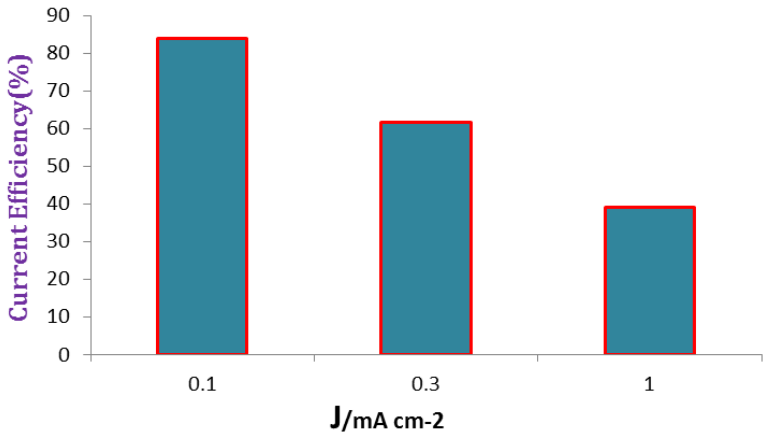

Fig. S2. Variation of current efficiency in the synthesis of **2NPAC** versus applied current density. Charge consumed=50 C.

Fig. S3 shows the effect of current density on the generated potential during constant-current synthesis of **2NOAC**. This Fig. shows that when the current density, 0.15 mA/cm^2 was selected as an optimum current density. Our data show that, the highest product yield (64%) was obtained at current density of 0.15 mA/ cm^2.

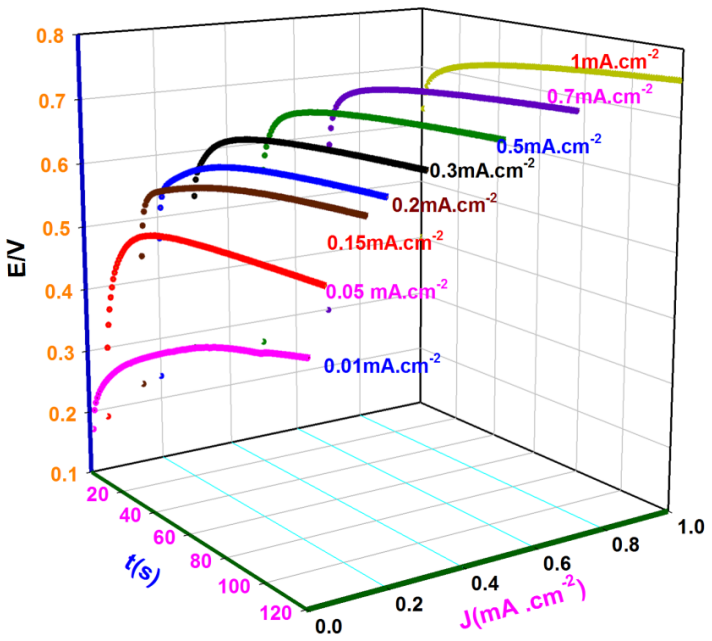

Fig. S3. The potential-time diagram during constant current electrolysis of **OAC** (0.25 mmol) in the presence of nitrite ion (1 mmol), at glassy carbon electrode in acetate buffer solution (pH = 5.0, *c* = 0.2 M). Rotation rate: 1000 rpm. Temperature = 25±1 ˚C.

The current efficiency for various current densities during the synthesis of **2NOAC** is shown in Fig. S4. The current density varied from 0.05 to 1.0 mA/cm^2, while the other parameters are kept constant. The effect of current density on the current efficiency is shown in Fig. S4.

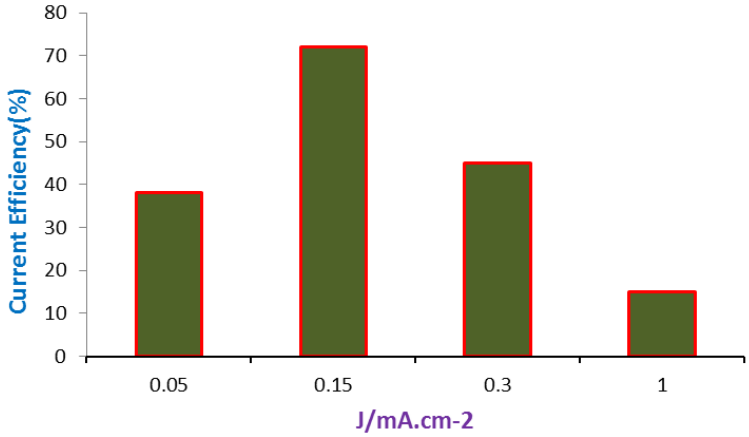

Fig. S4. Variation of current efficiency in the synthesis of **2NOAC** versus applied current density. Charge consumed=50 C.

Fig. S5 shows the effect of current density on the generated potential during constant-current synthesis of **2NAPIP**. This Fig. shows that when the current density, 0.25 mA/cm^2 was selected as an optimum current density. Our data show that, the highest product yield (75%) was obtained at current density of 0.15 mA/ cm^2.

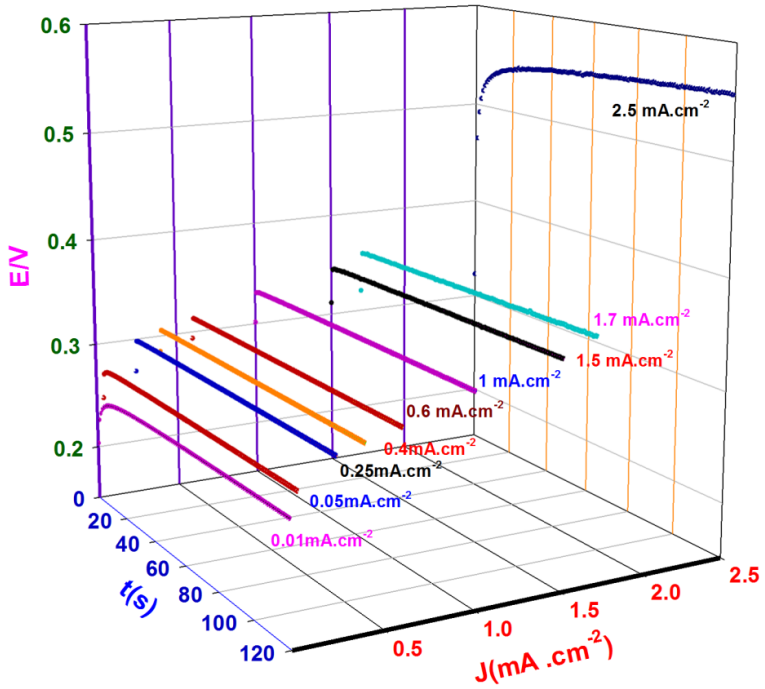

Fig. S5. The potential-time diagram during constant current electrolysis of **APIP** (0.25 mmol) in the presence of nitrite ion (1 mmol), at glassy carbon electrode in acetate buffer solution (pH = 5.0, *c* = 0.2 M). Rotation rate: 1000 rpm. Temperature = 25±1 ◦C.

The current efficiency for various current densities during the synthesis of **2NAPIP** is shown in Fig. S6. The current density varied from 0.05 to 2.5 mA/cm^2, while the other parameters are kept constant. The effect of current density on the current efficiency is shown in Fig. S6.

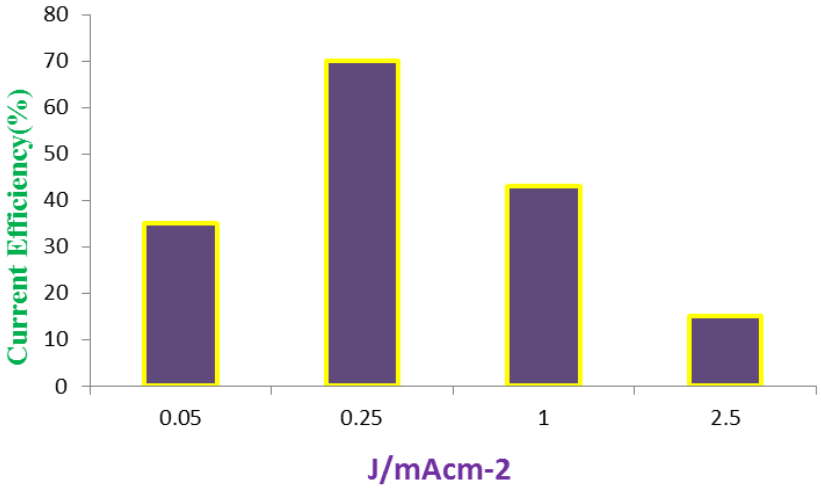

Fig. S6. Variation of current efficiency of the synthesis of **2NAPIP** versus applied current density. Charge consumed=50 C.

FTIR spectrum of 2NPAC

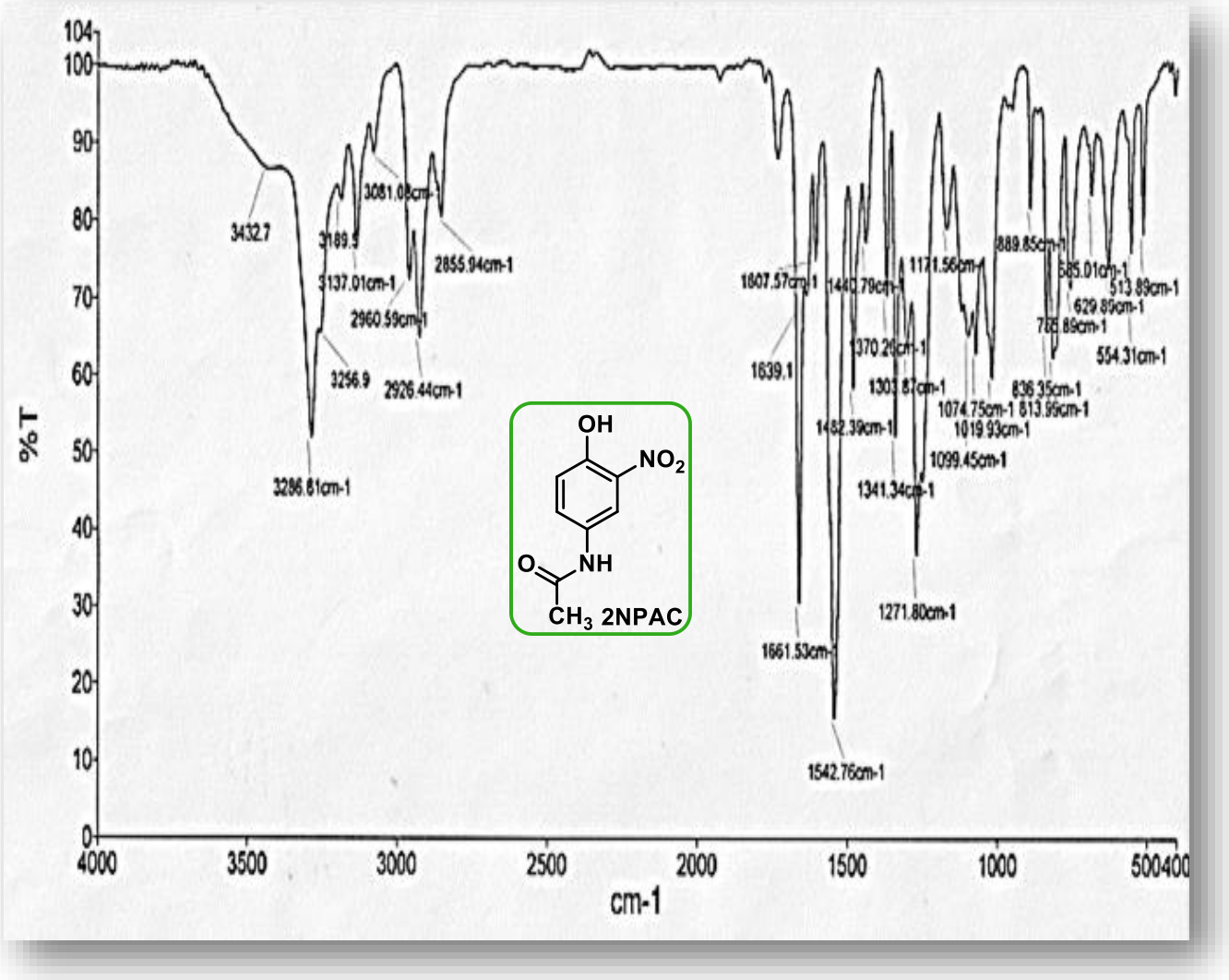

Mass spectrum of 2NPAC

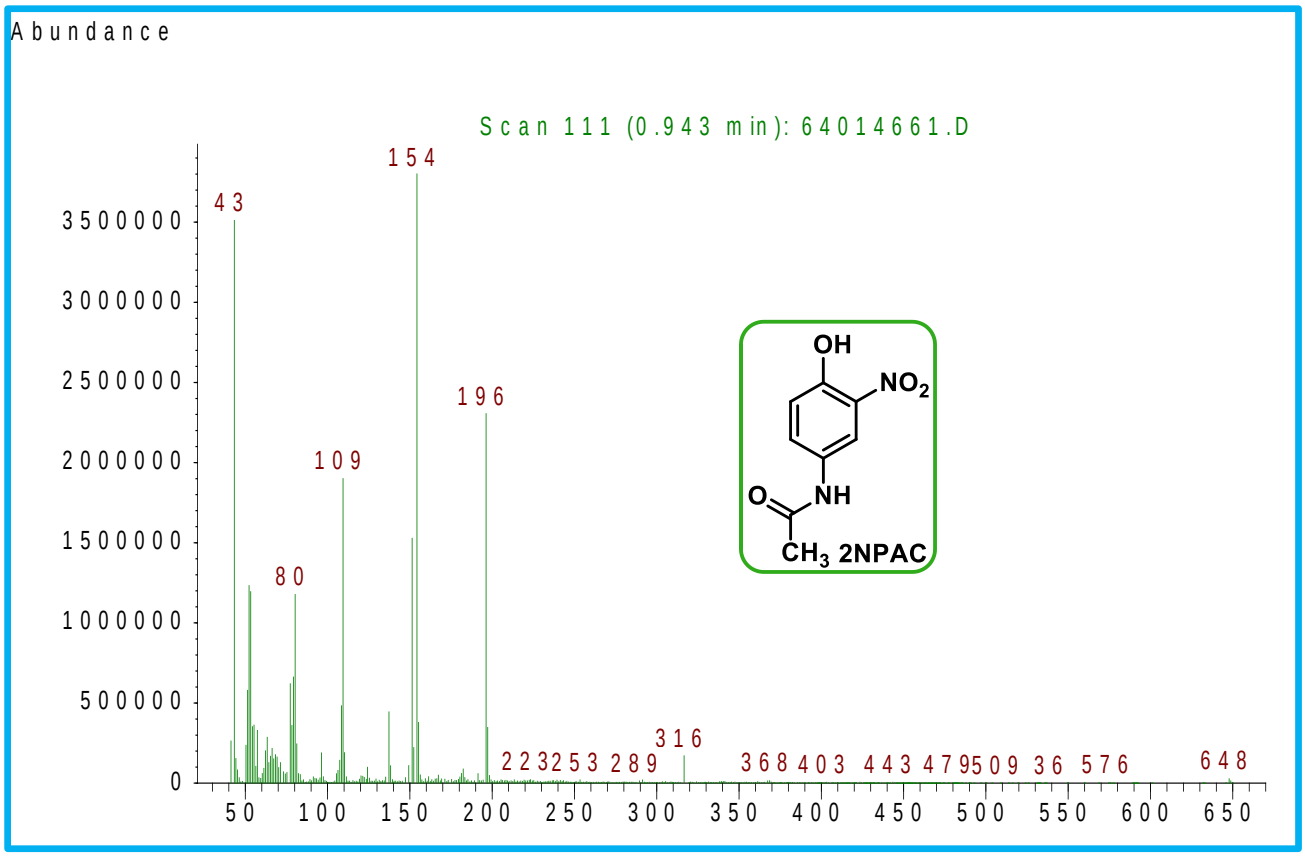

^{1}H NMR spectrum of 2NPAC

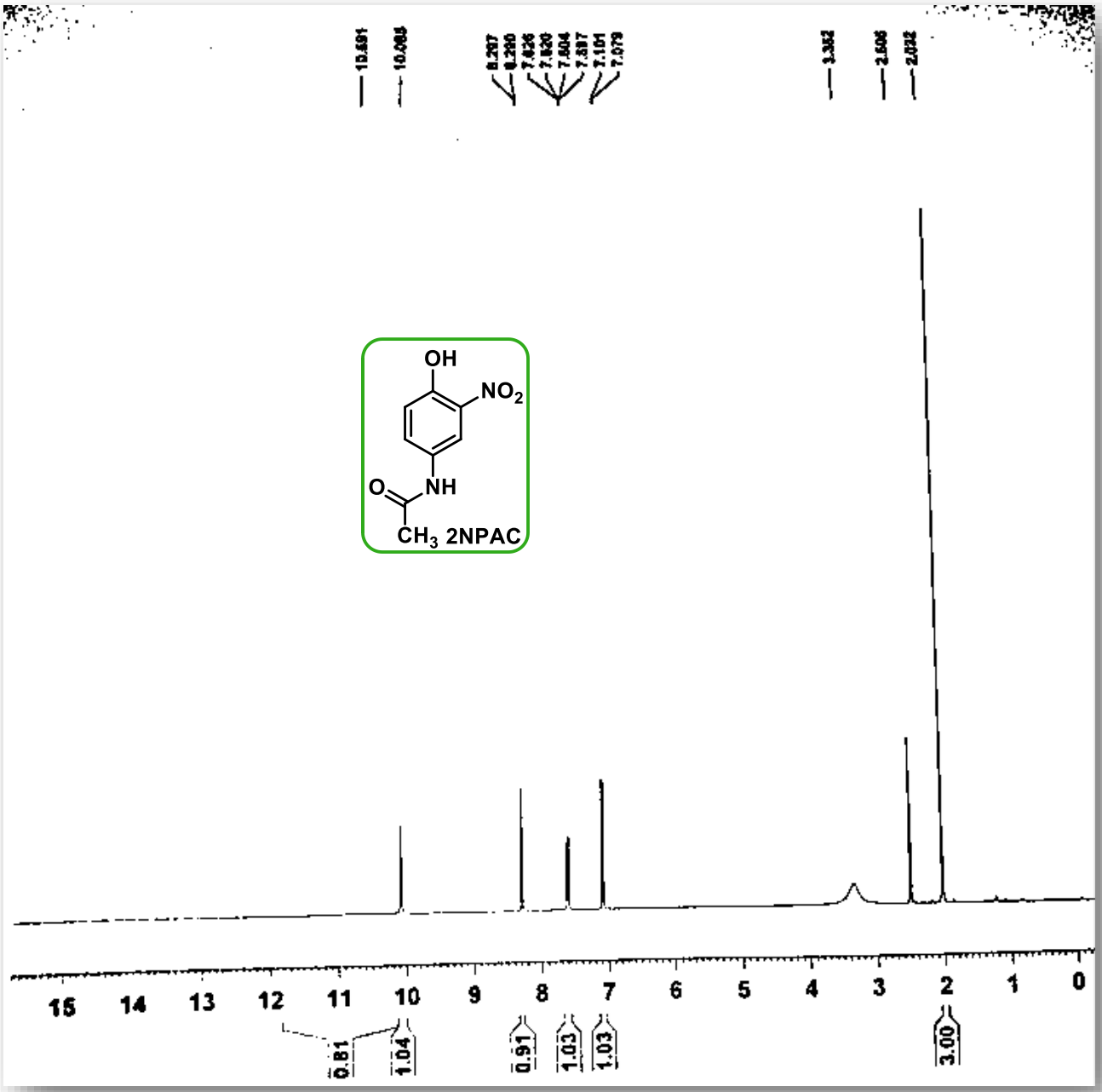

Expanded ^{1}H NMR spectrum of 2NPAC

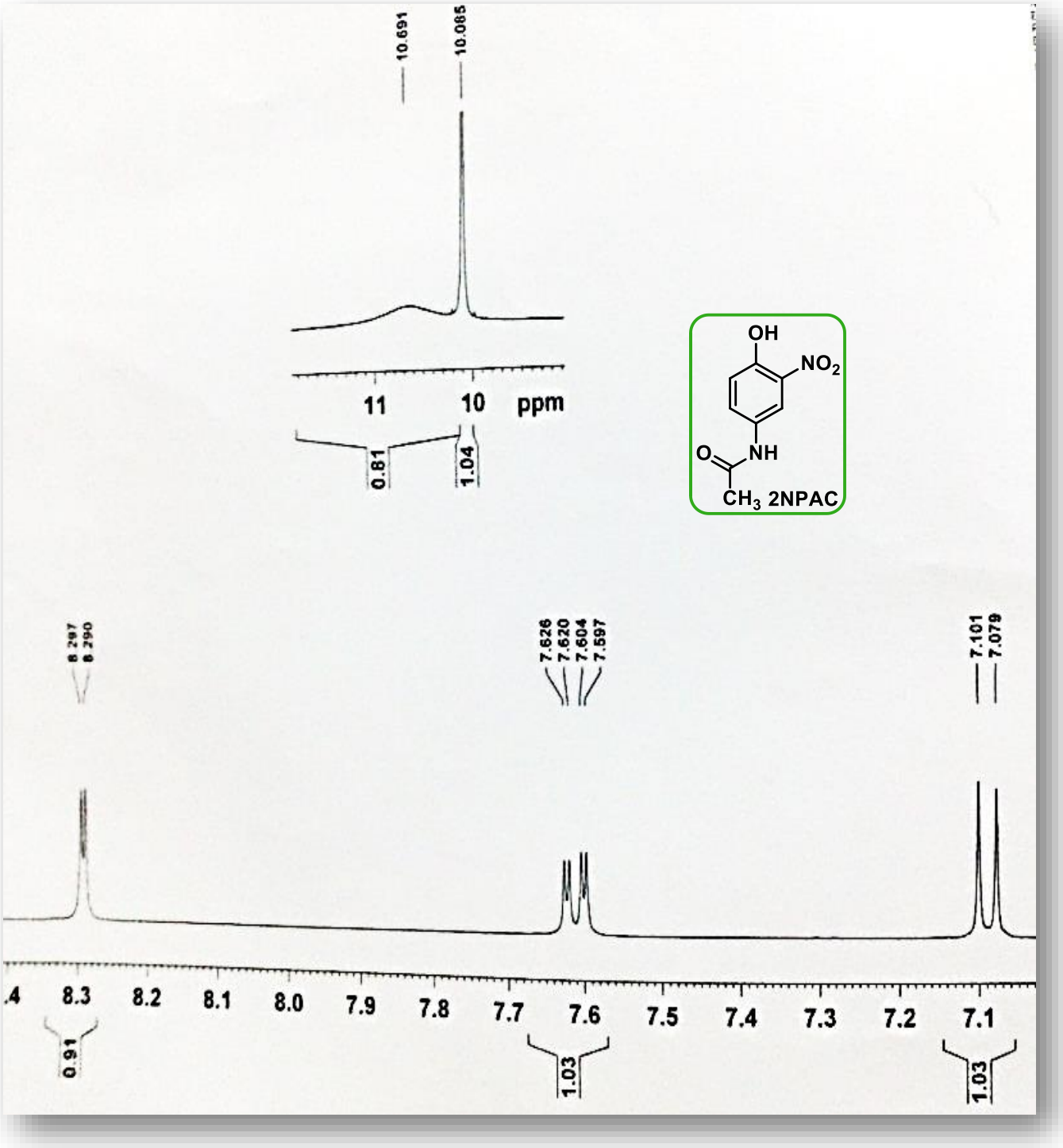

^{13}C NMR spectrum of 2NPAC

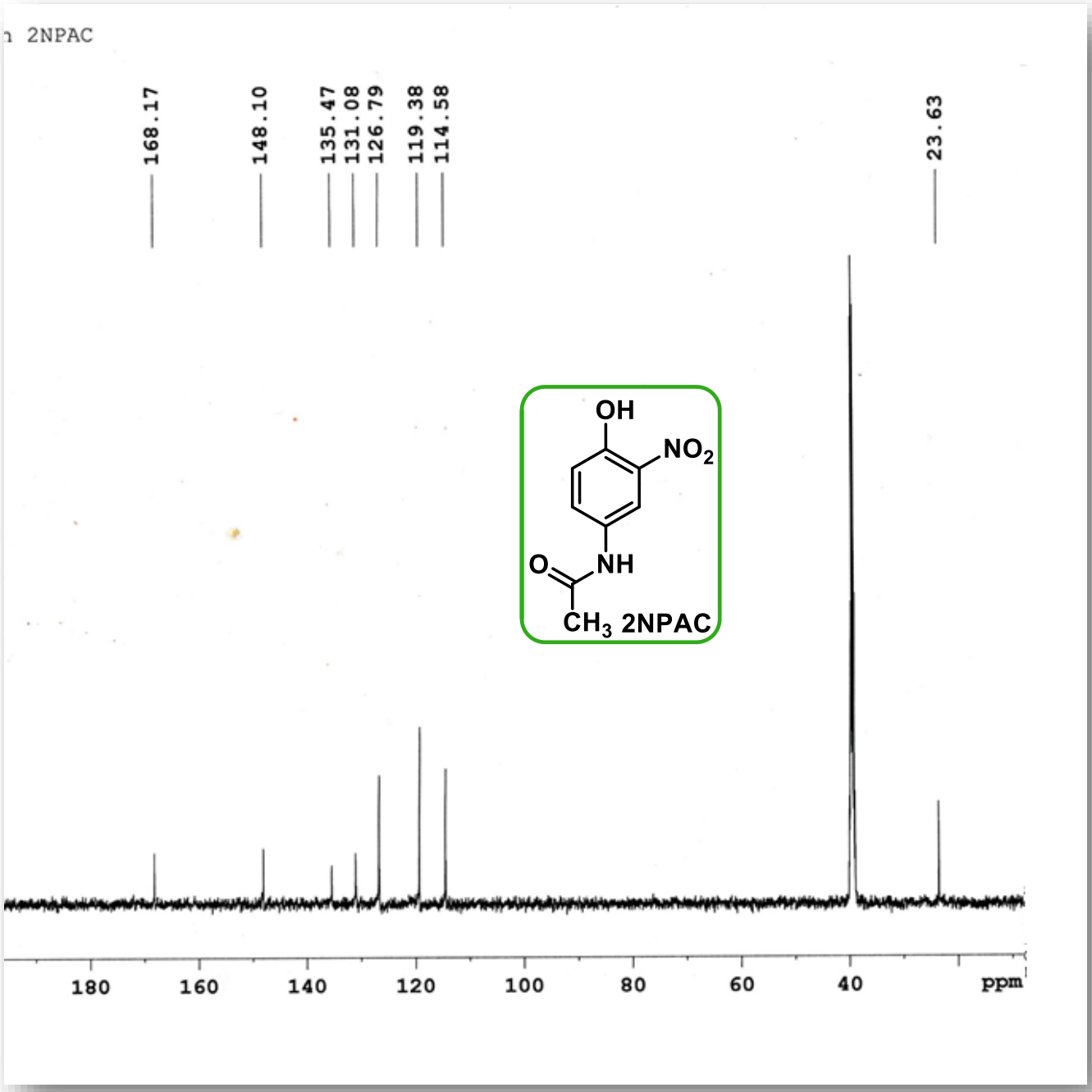

Expanded ^{13}C NMR spectrum of 2NPAC

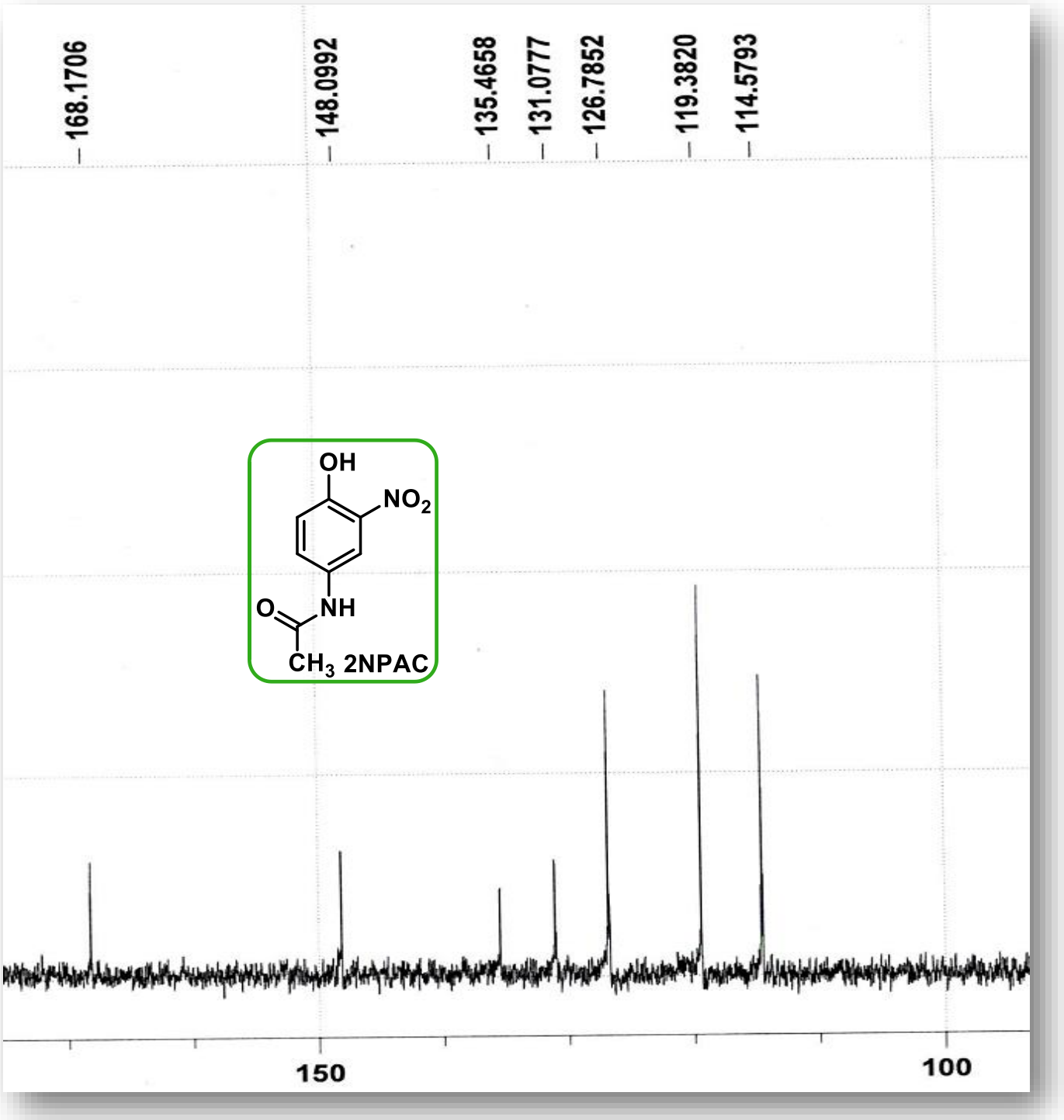

Thin layer chromatography of 2NPAC (electrochemical synthesis)

Silica gel: Ethyl acetate/*n*-Hexane (2/1 v/v)

Thin layer chromatography of 2NPAC (chemical synthesis)

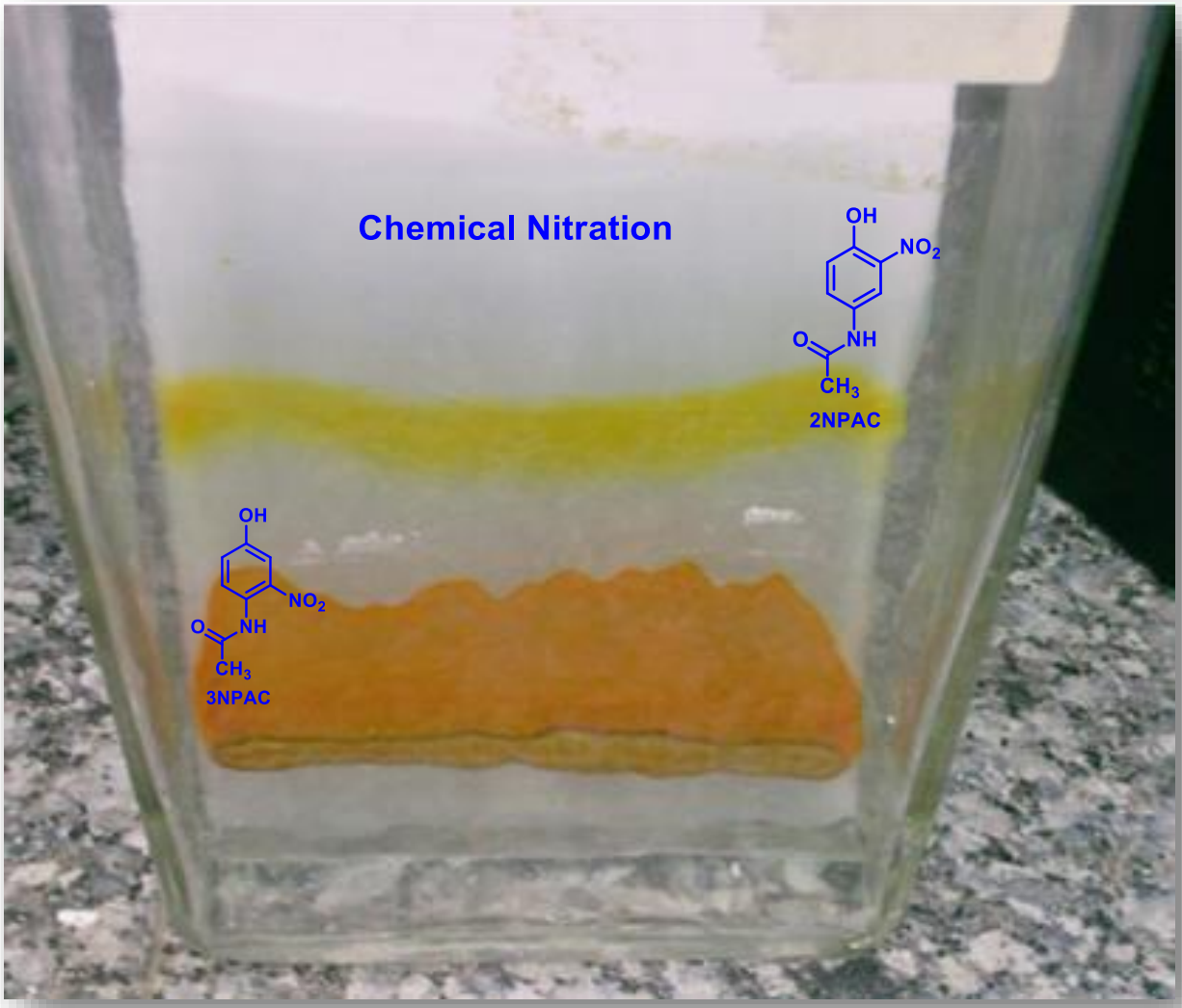

FT-IR spectra of 2NPAC and 3NPAC obtained from chemical synthesis

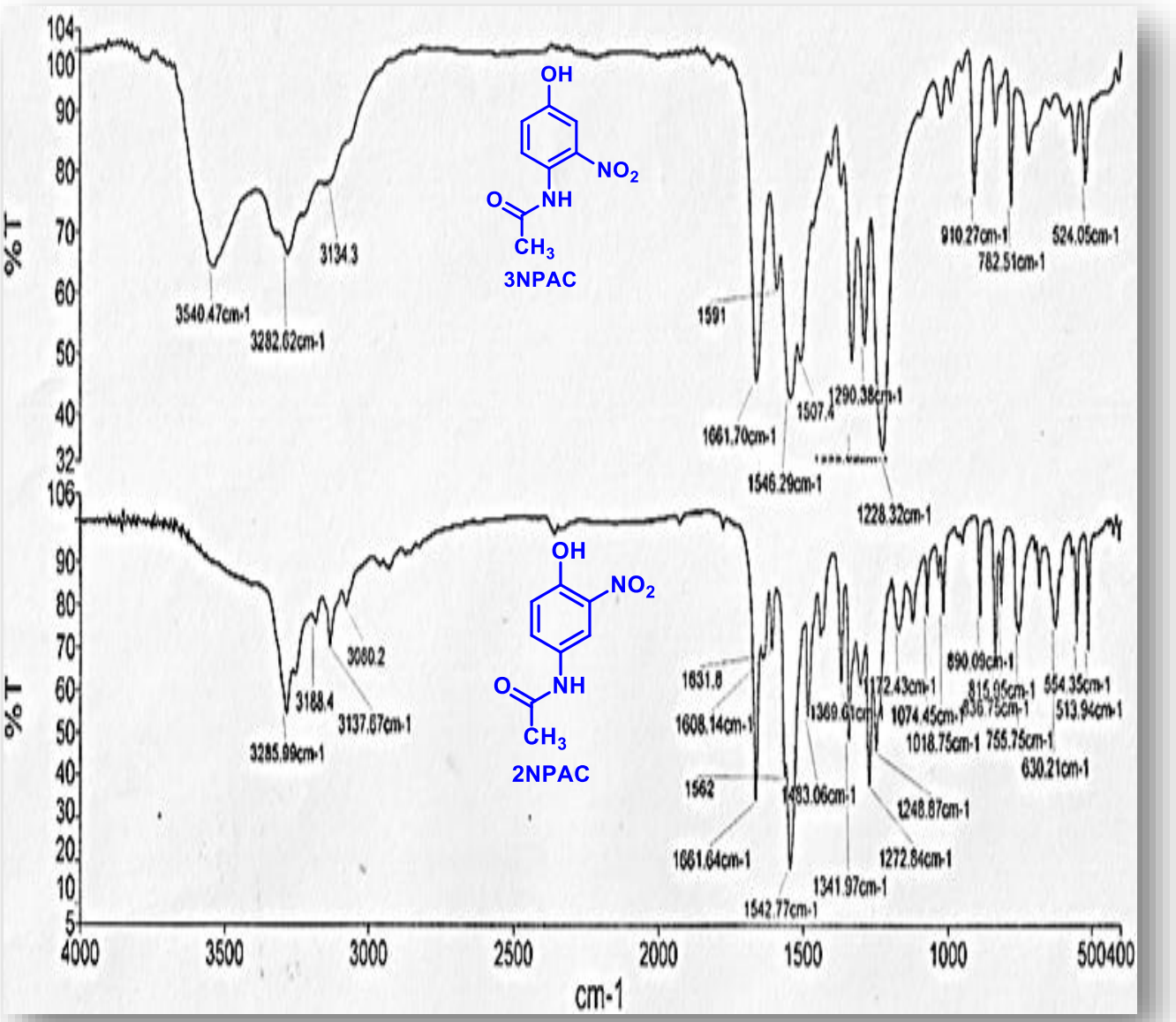

Mass spectrum of 3NPAC (chemical synthesis)

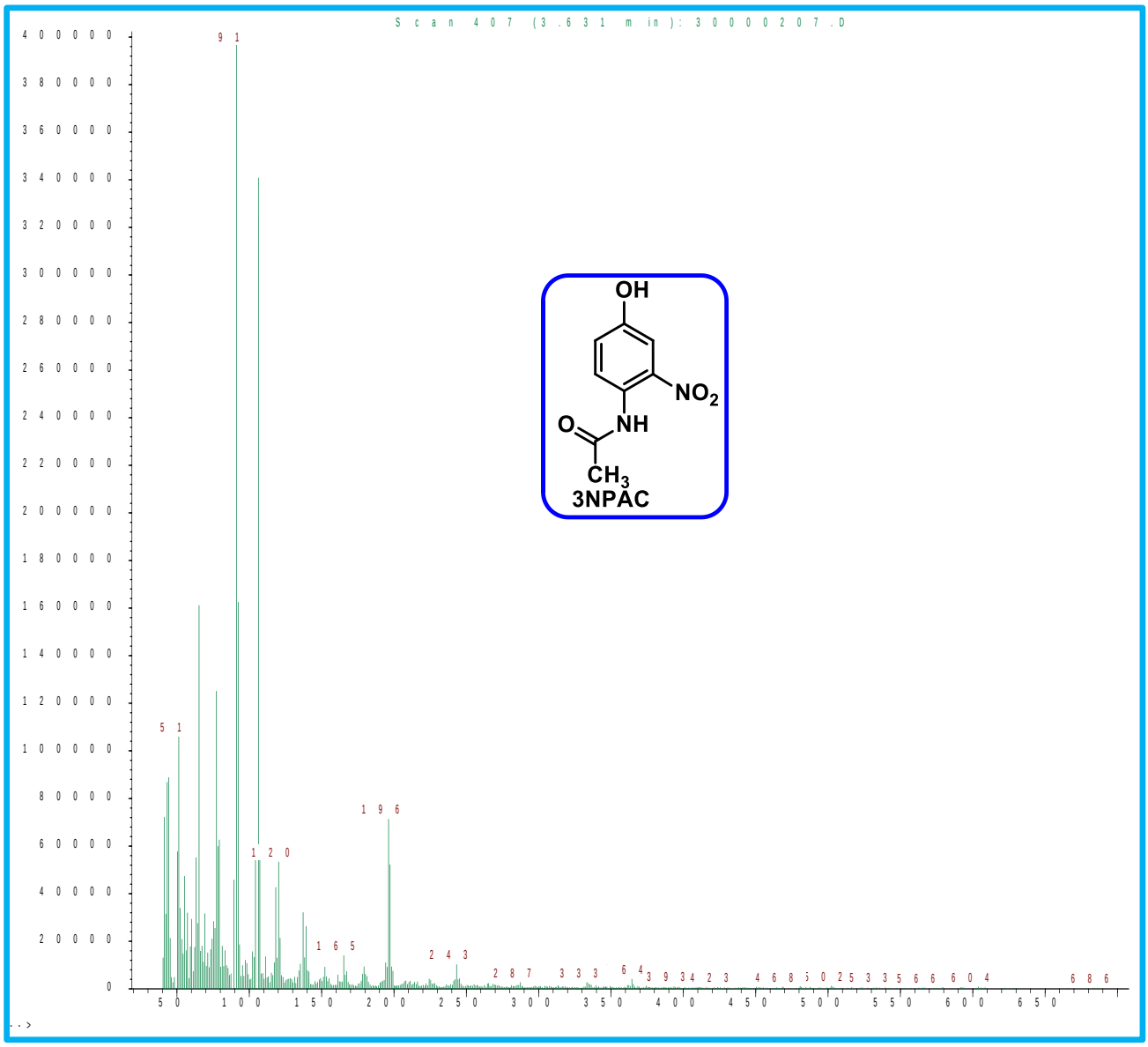

FT-IR spectra of 2NPAC synthesized from electrochemical & chemical methods

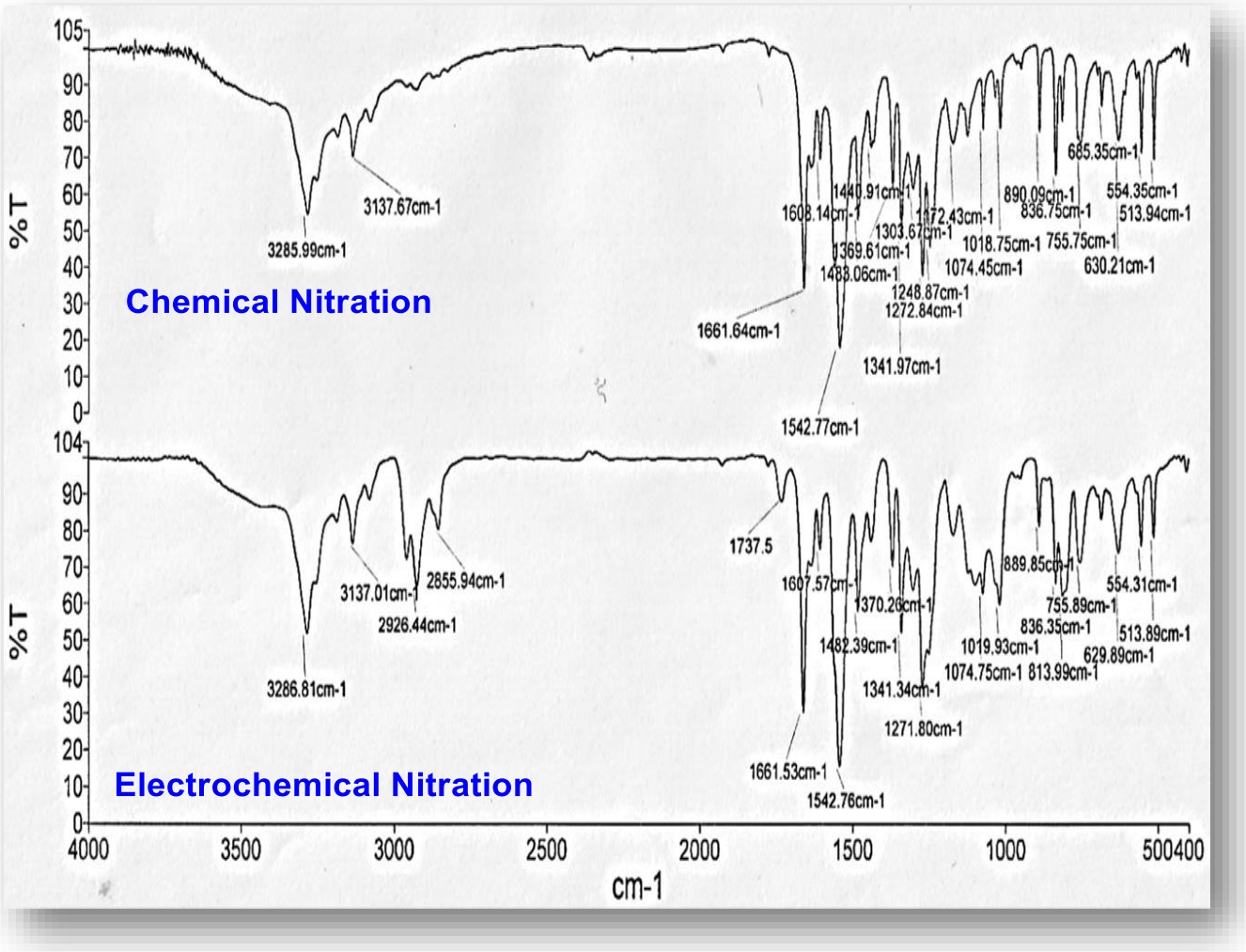

UV-Vis spectra of 2NPAC & 3NPAC (at pH=5.0)

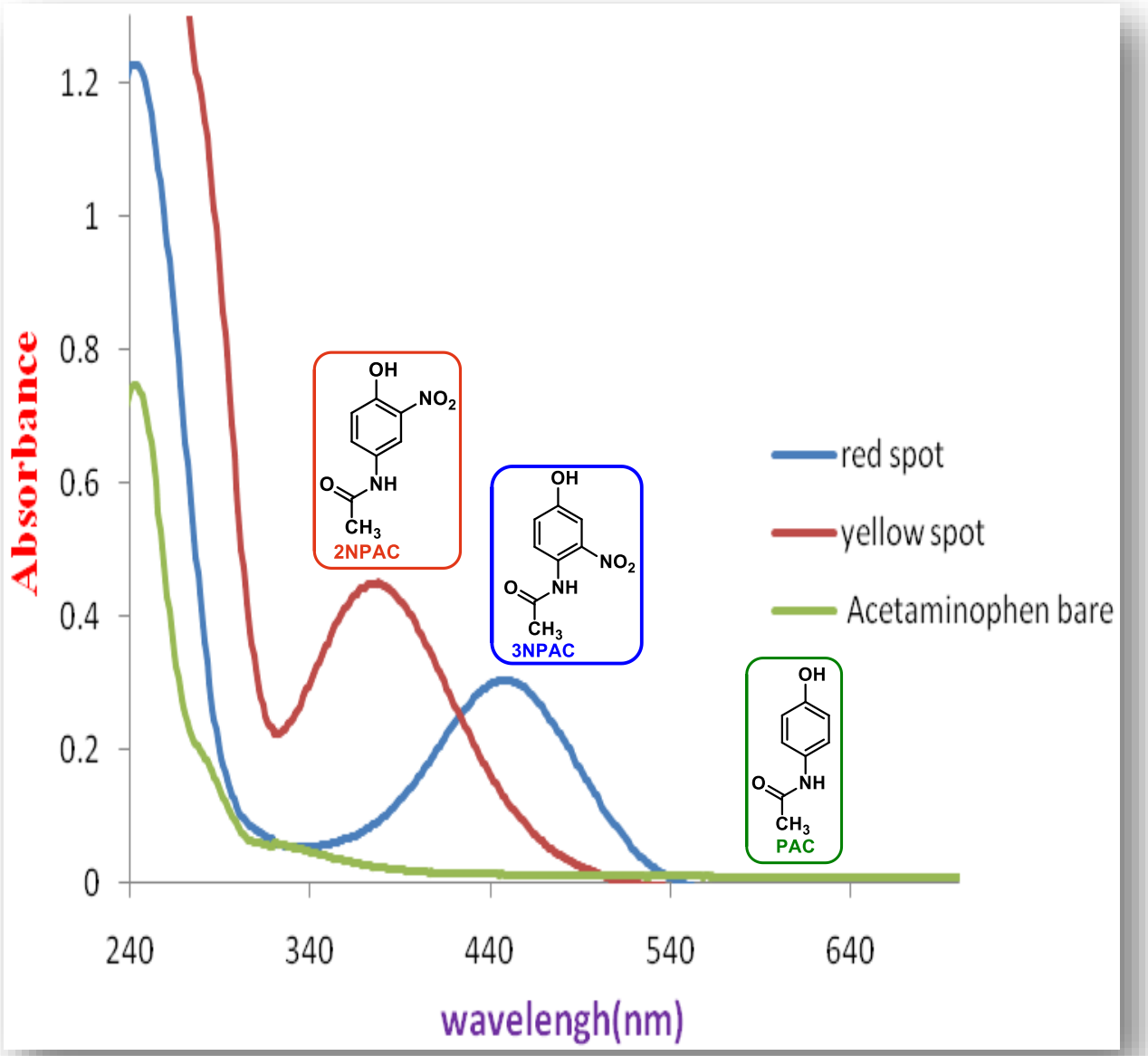

FTIR spectrum of 2NOAC

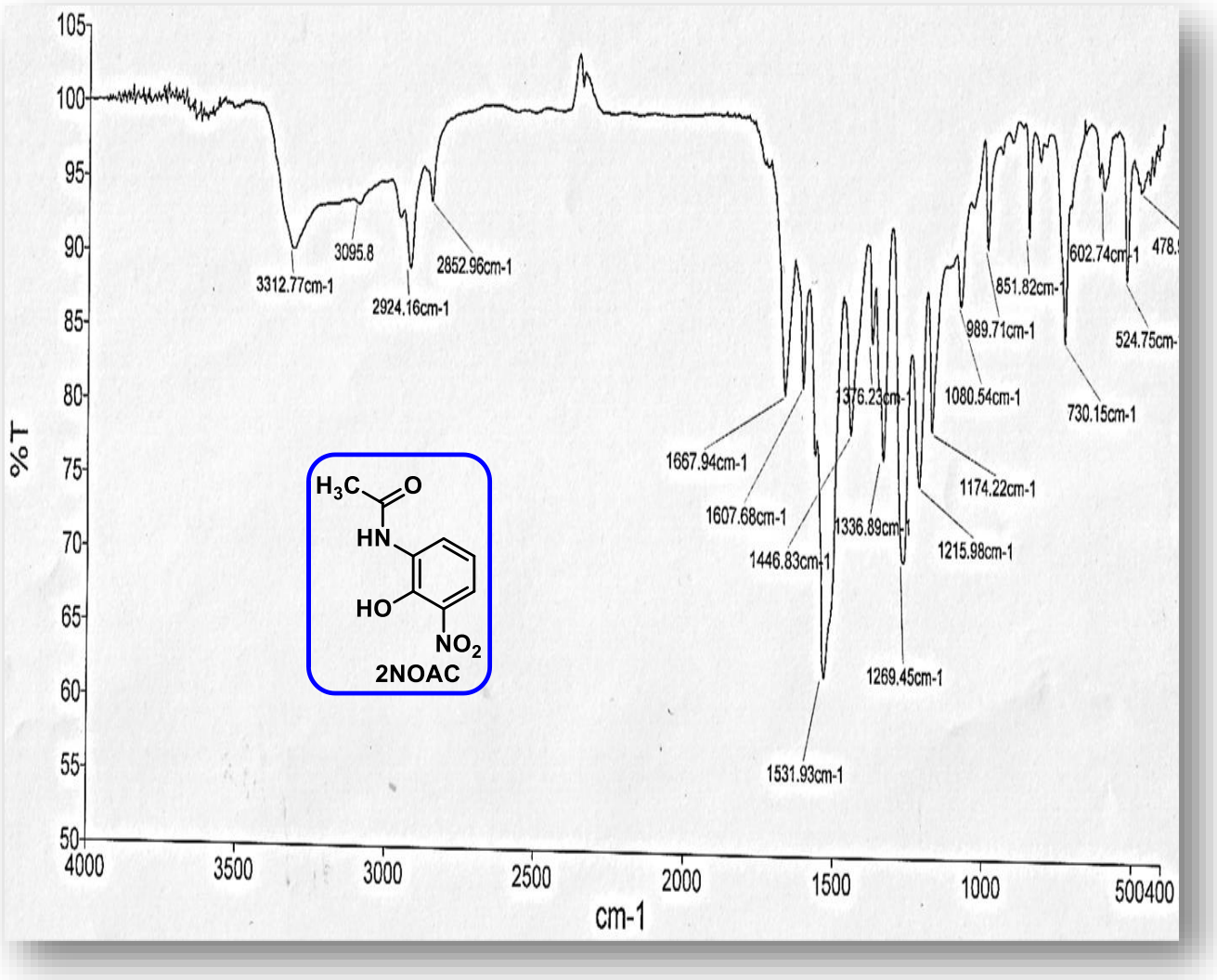

Mass spectrum of 2NOAC

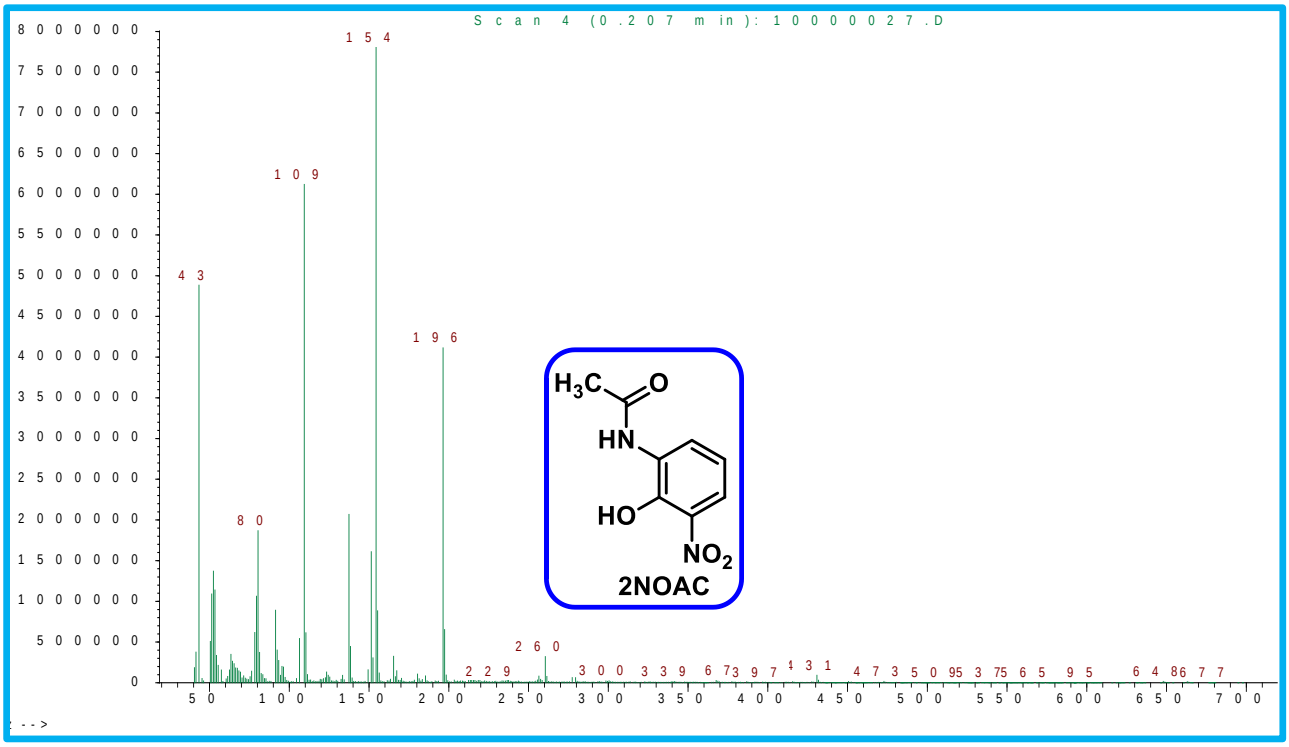

^{1}H NMR spectrum of 2NOAC

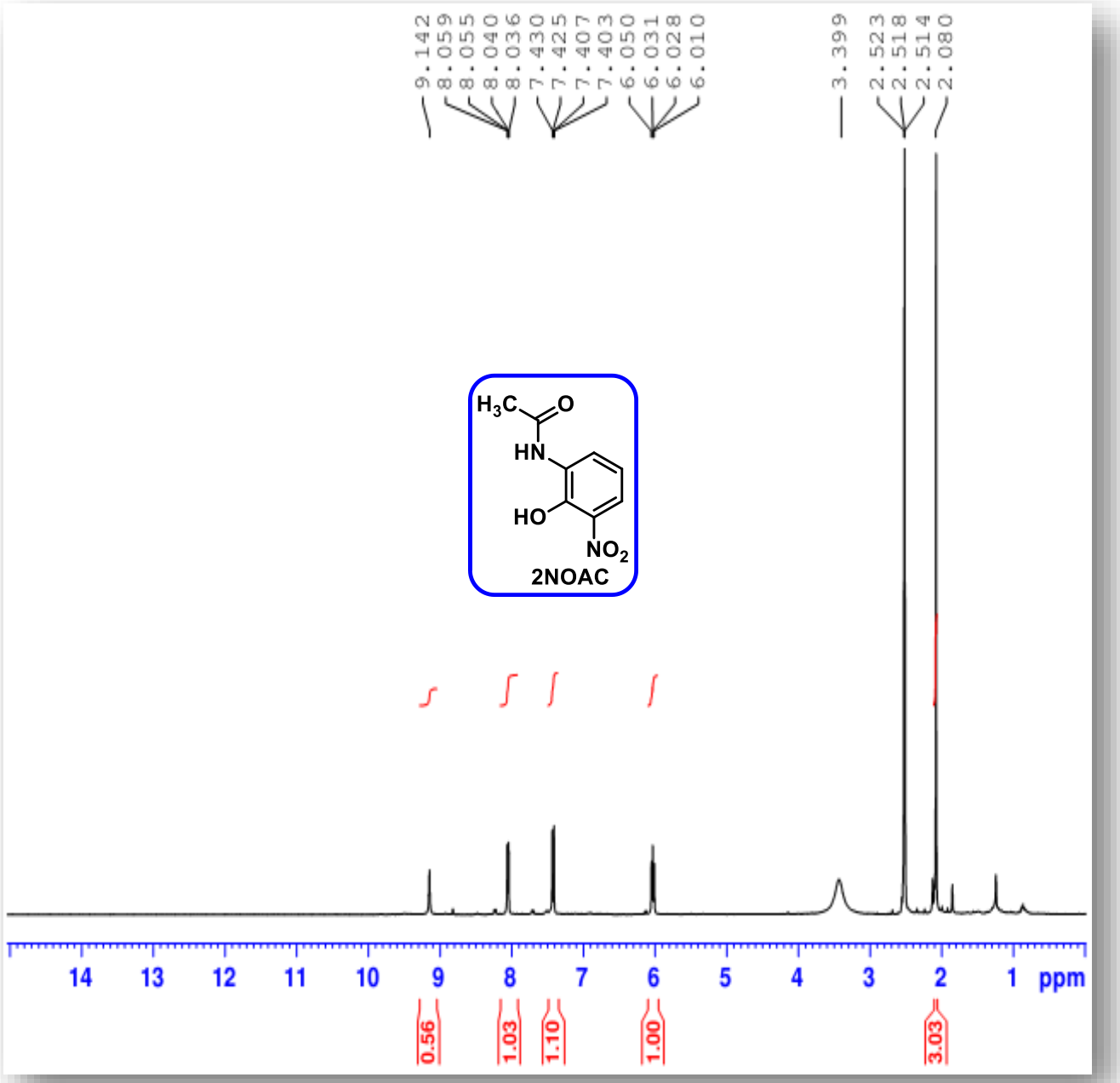

Expanded ^{1}H NMR spectrum of 2NOAC

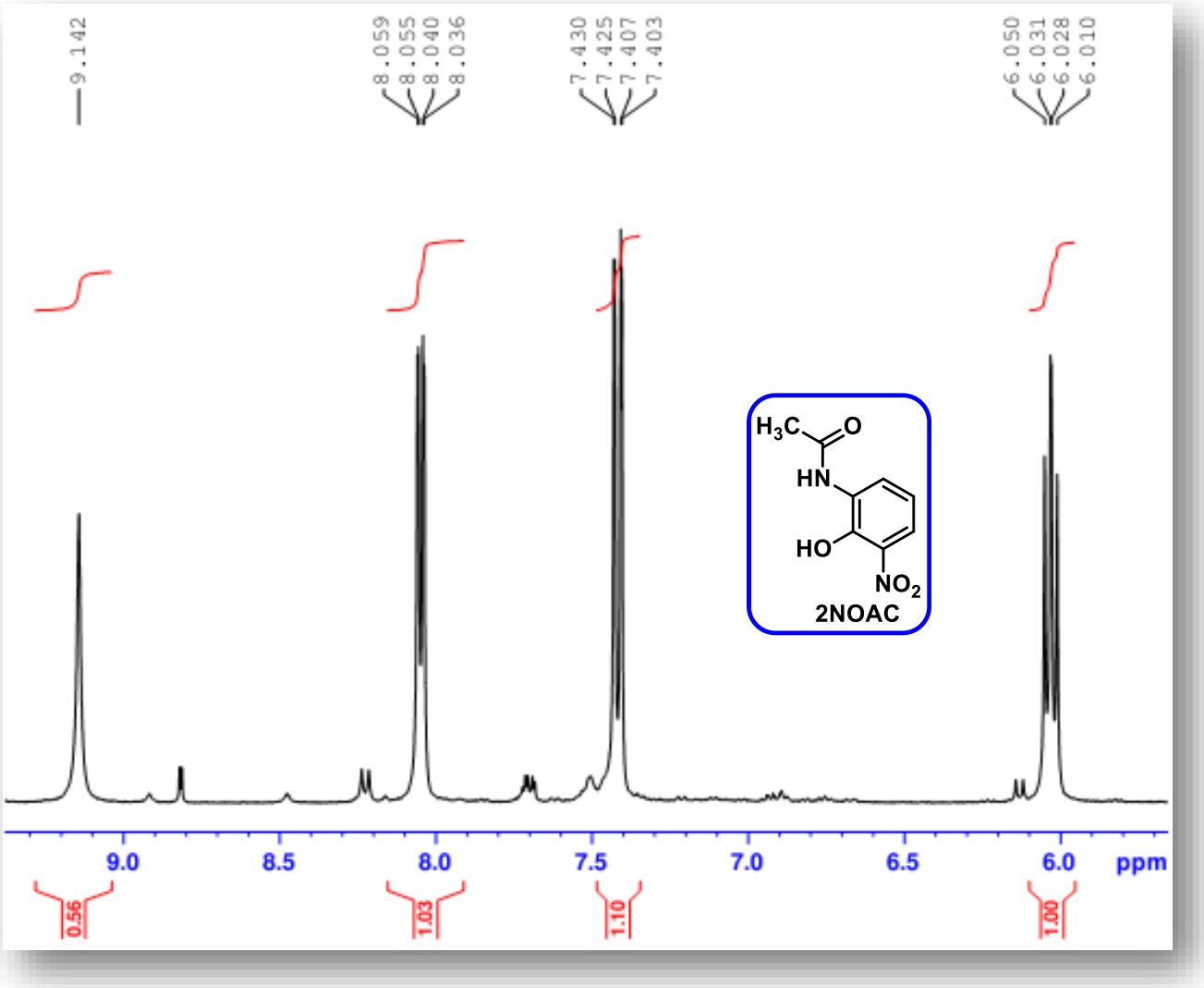

^{1}H NMR spectrum of 2NOAC (with D_2O)

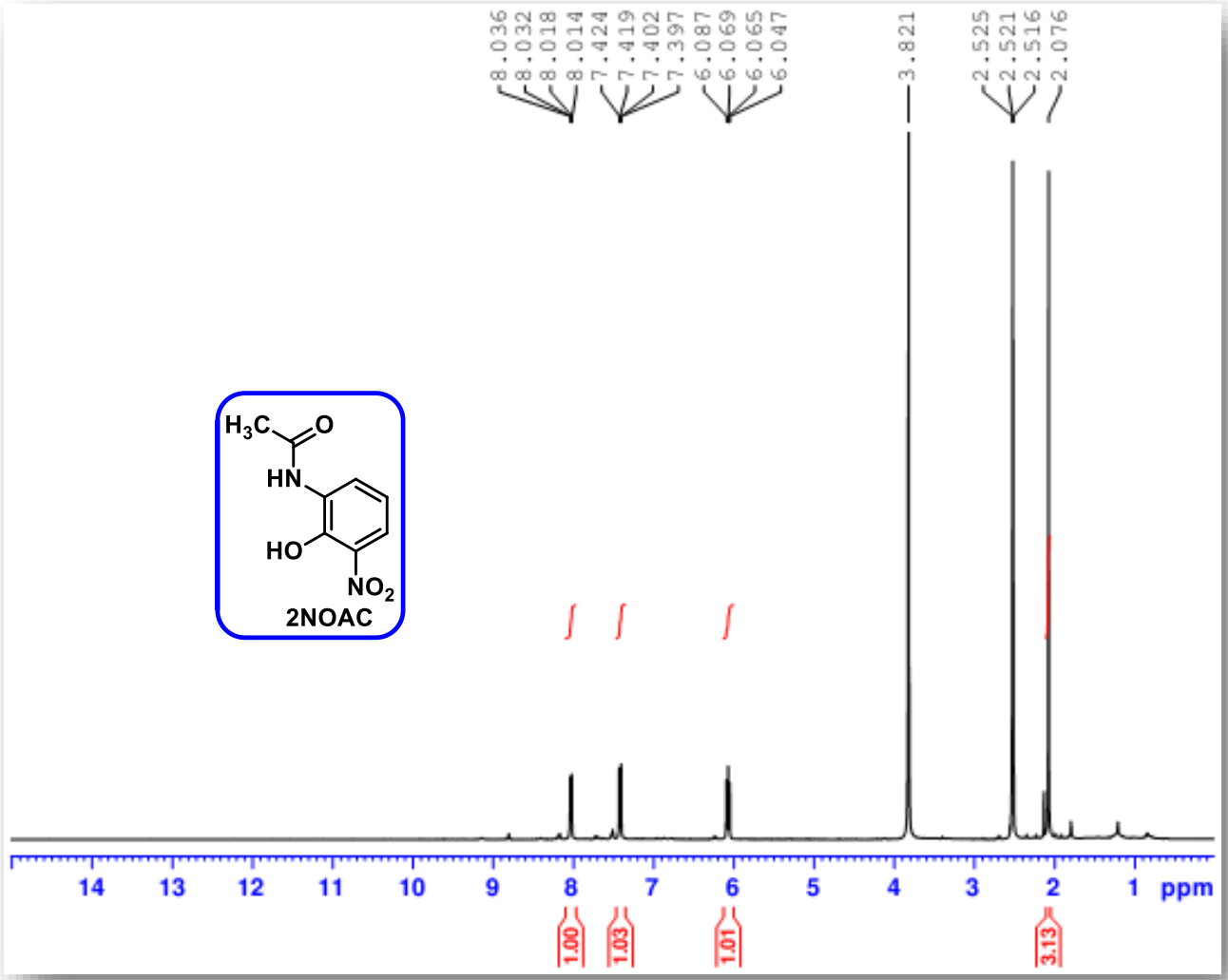

Expanded ^{1}H NMR spectrum of 2NOAC (with D_2O)

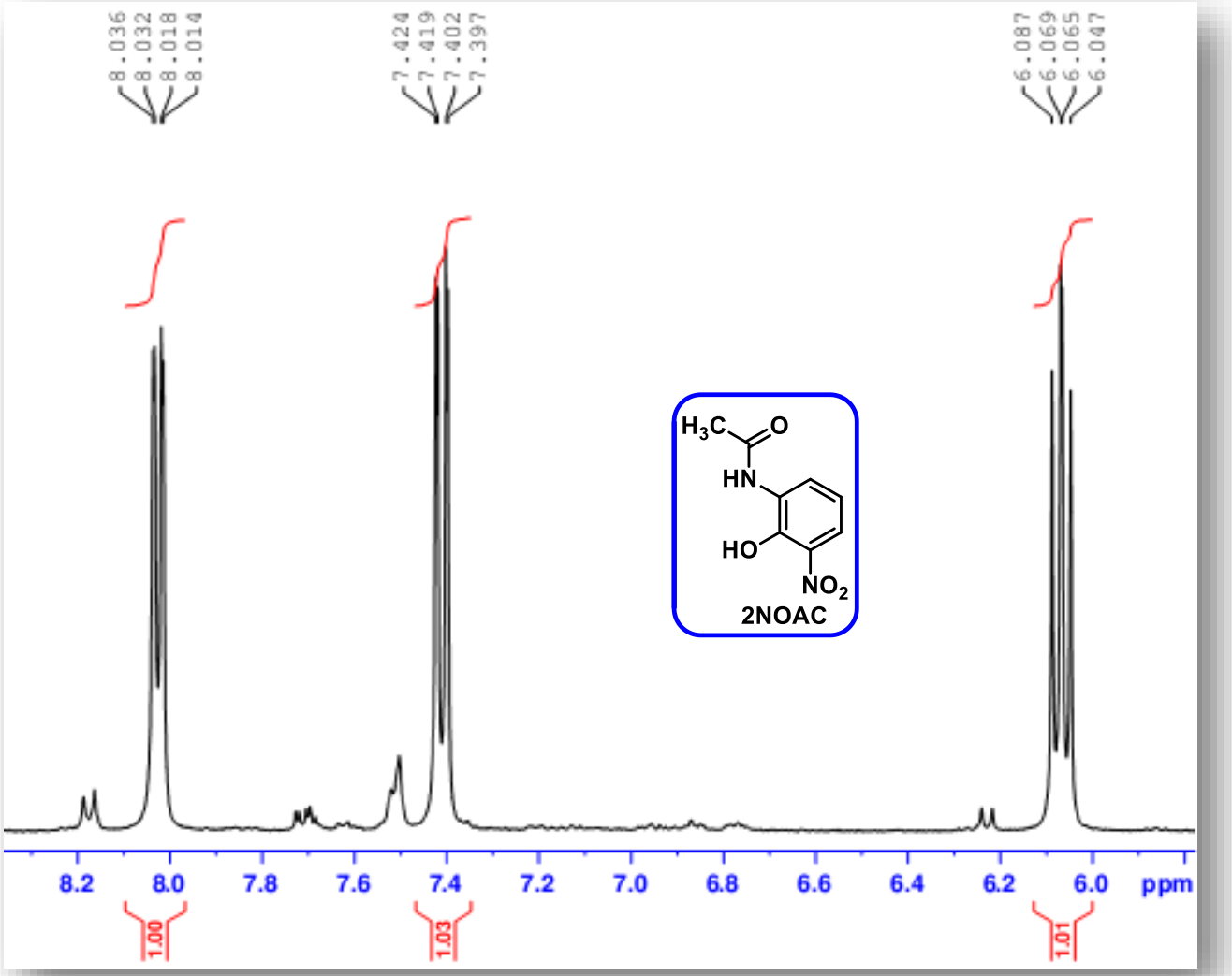

^{13}C NMR spectrum of 2NOAC

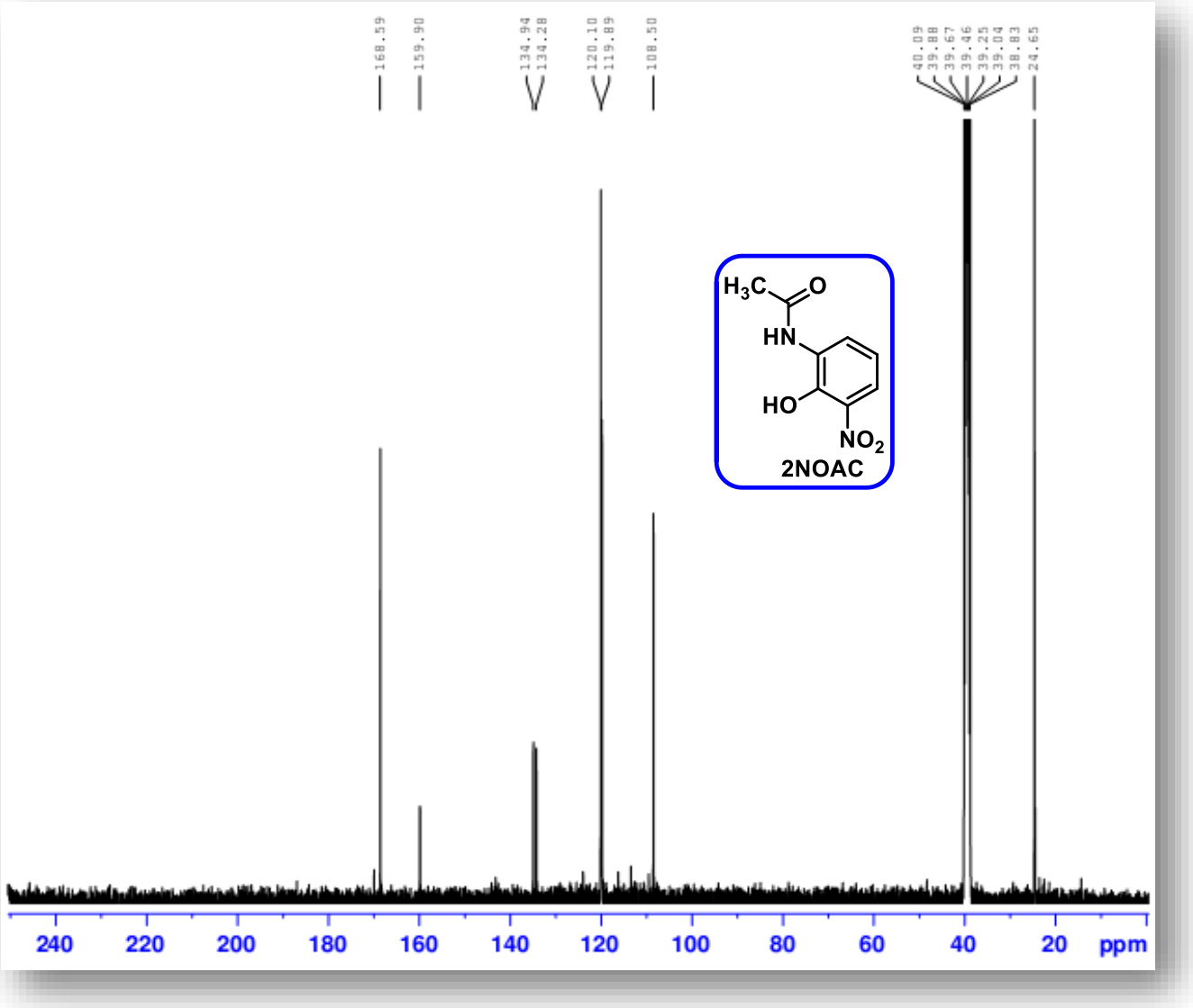

ORTEP view of X-ray crystal structure of 2NPAC

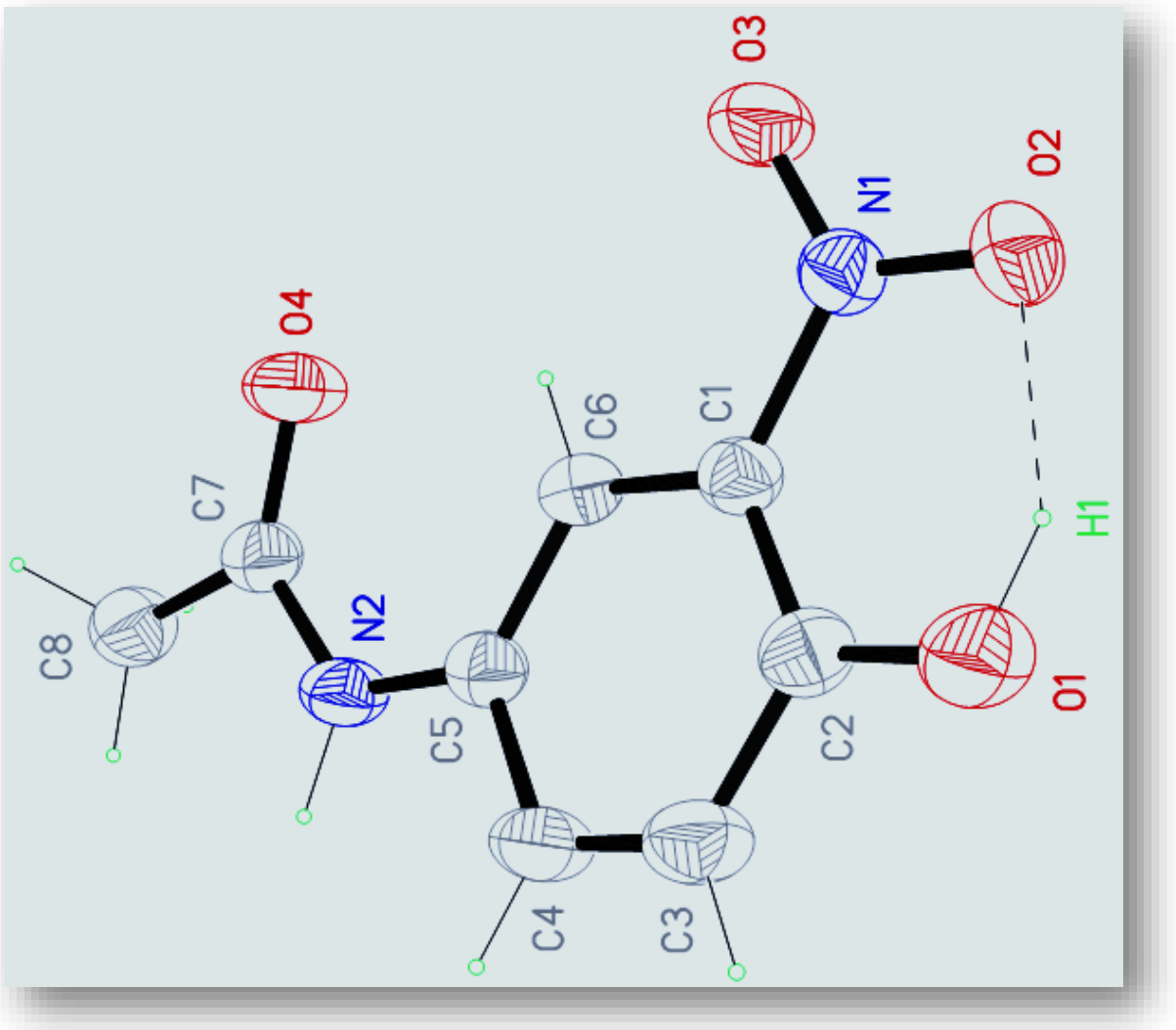

FTIR spectrum of 2NAPIP

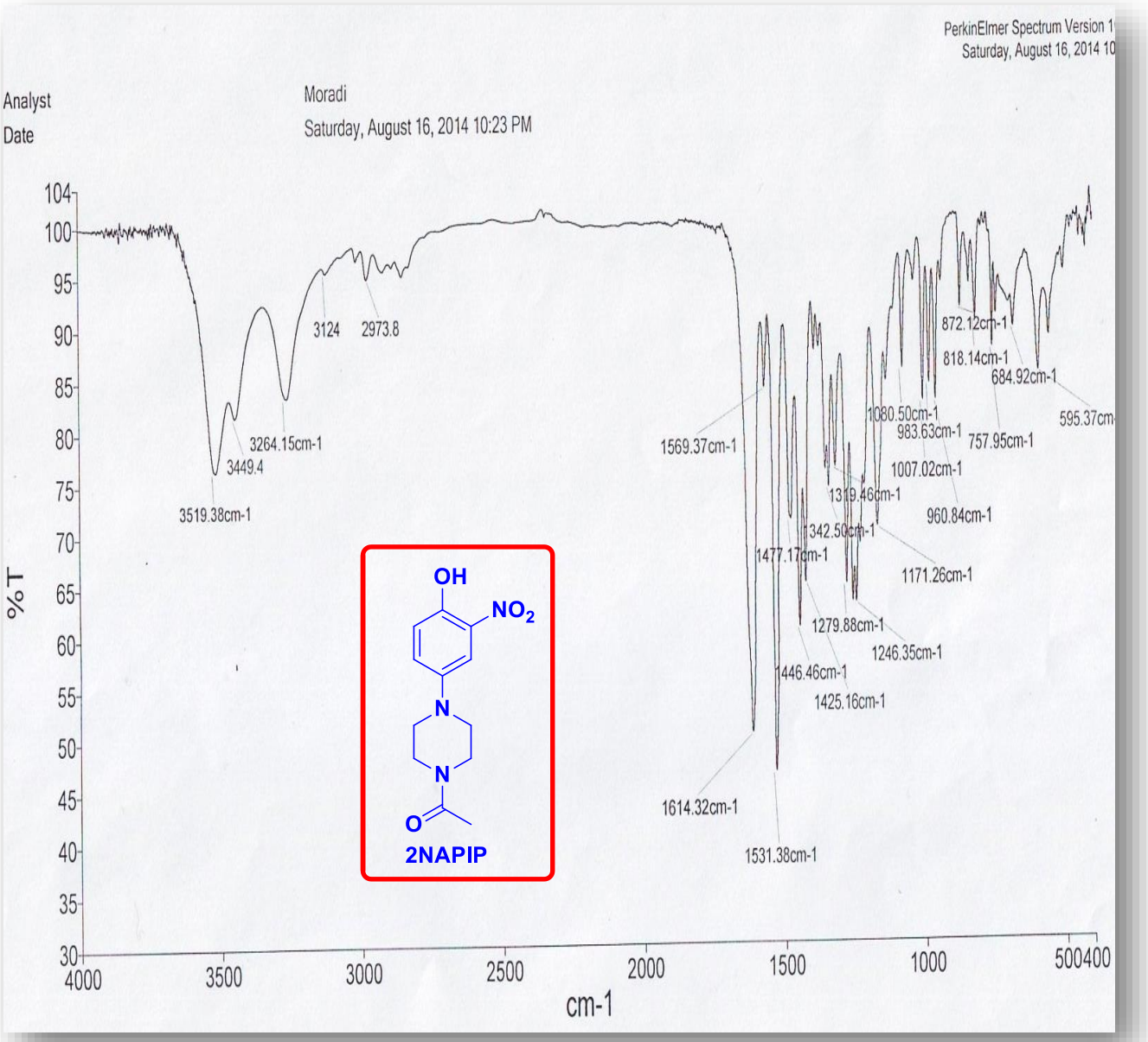

Mass spectrum of 2NAPIP

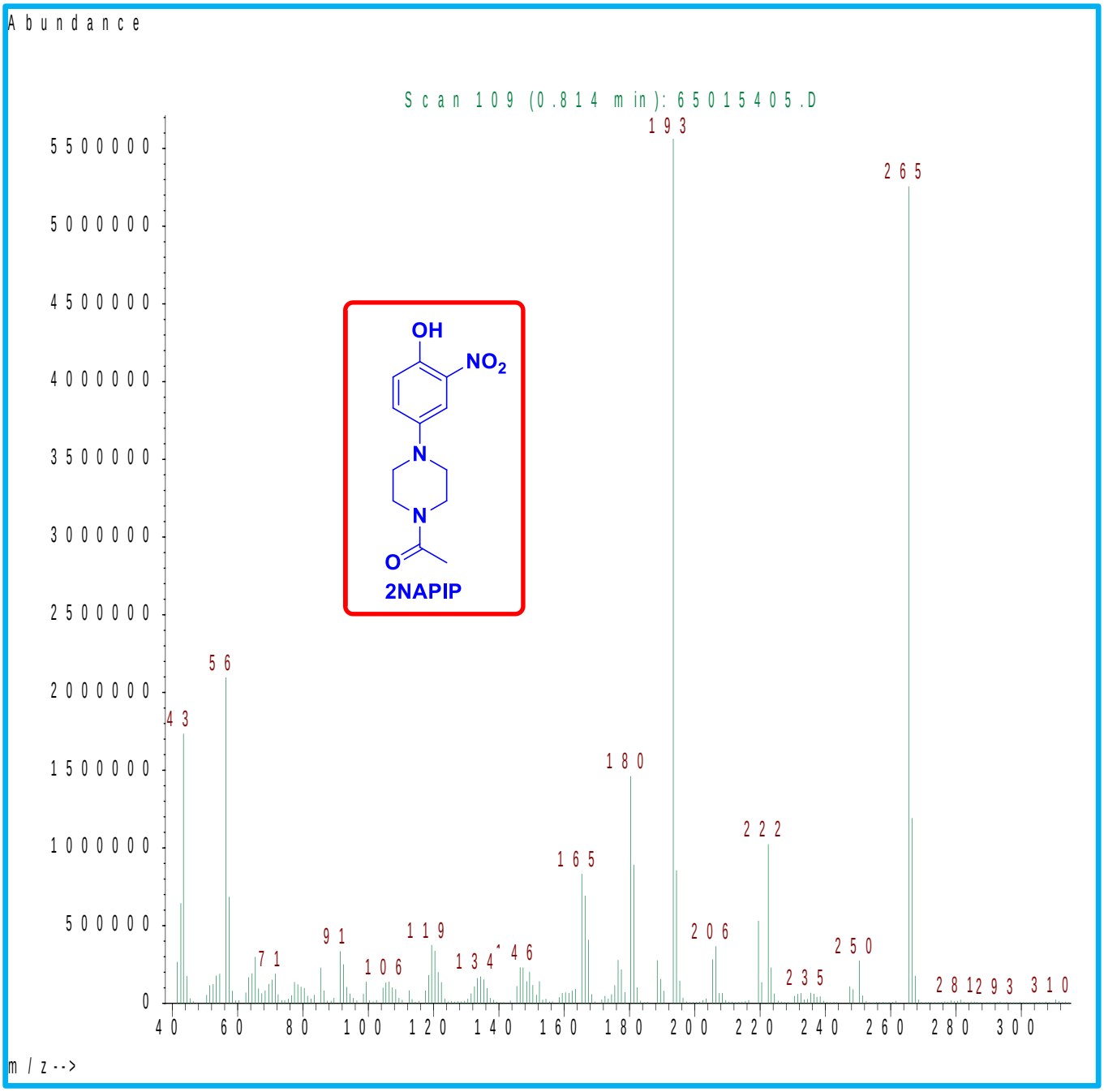

^{1}H NMR spectrum of 2NAPIP

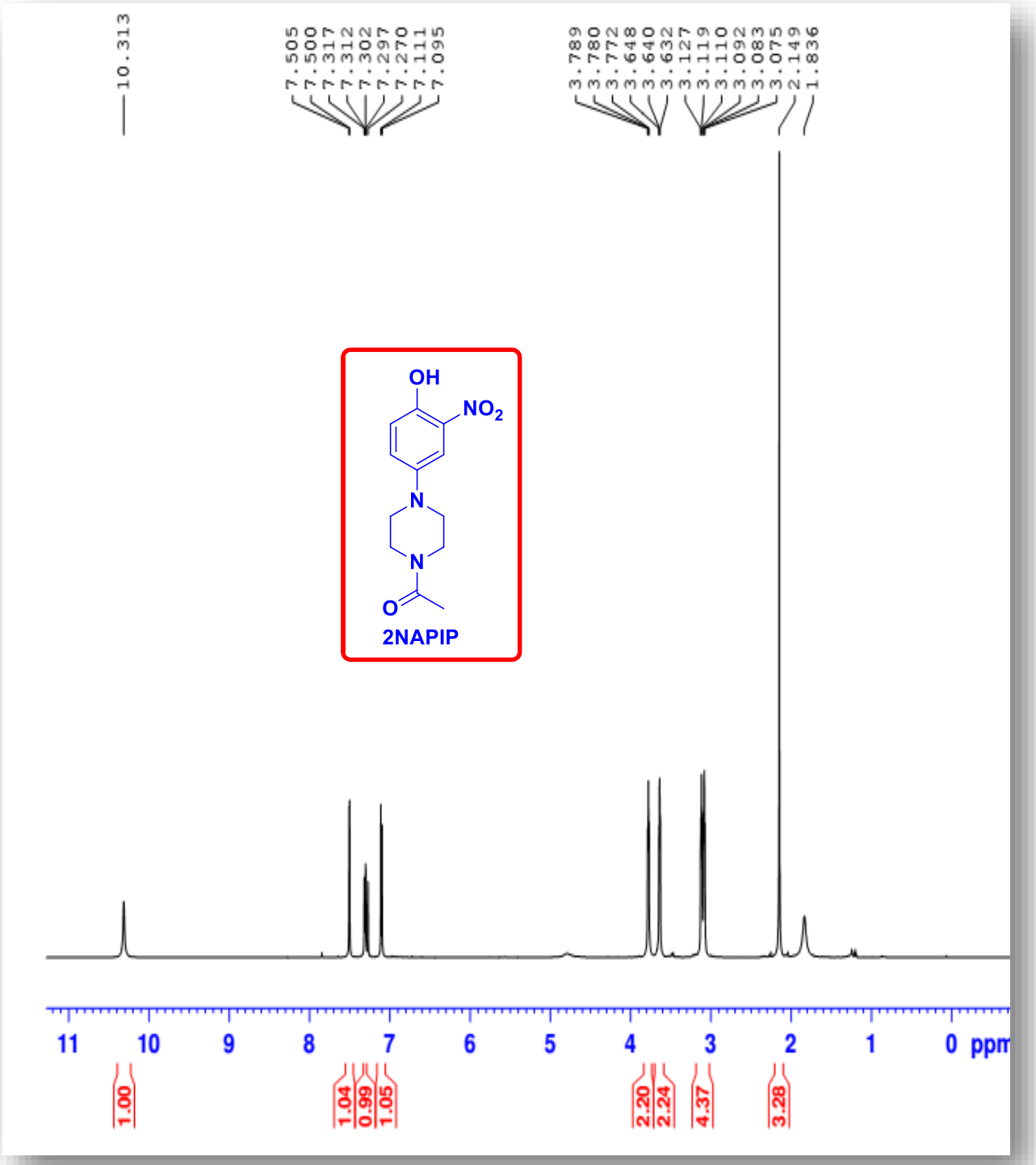

Expanded ^{1}H NMR spectrum of 2NAPIP

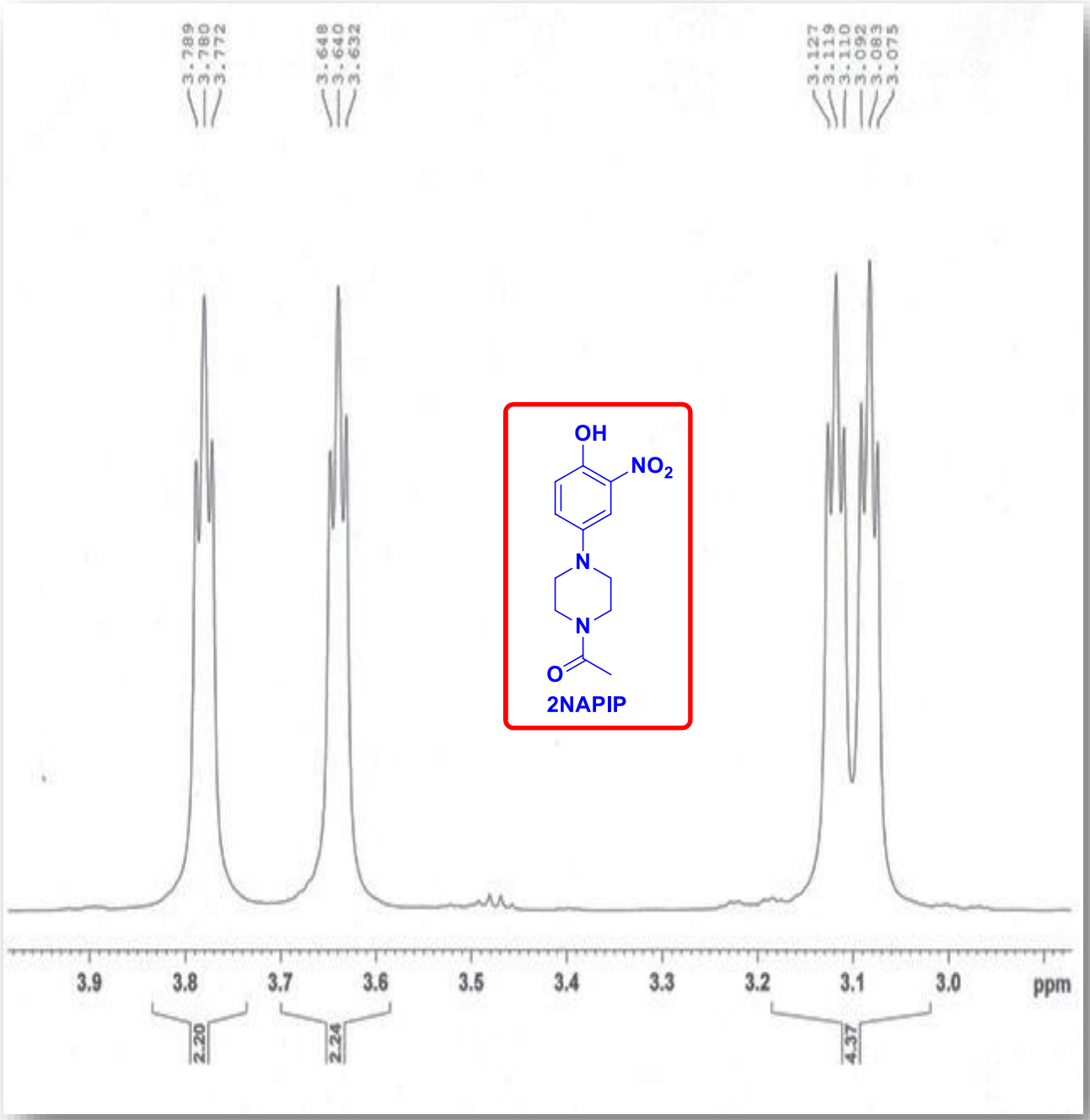

Expanded ^{1}H NMR spectrum of 2NAPIP

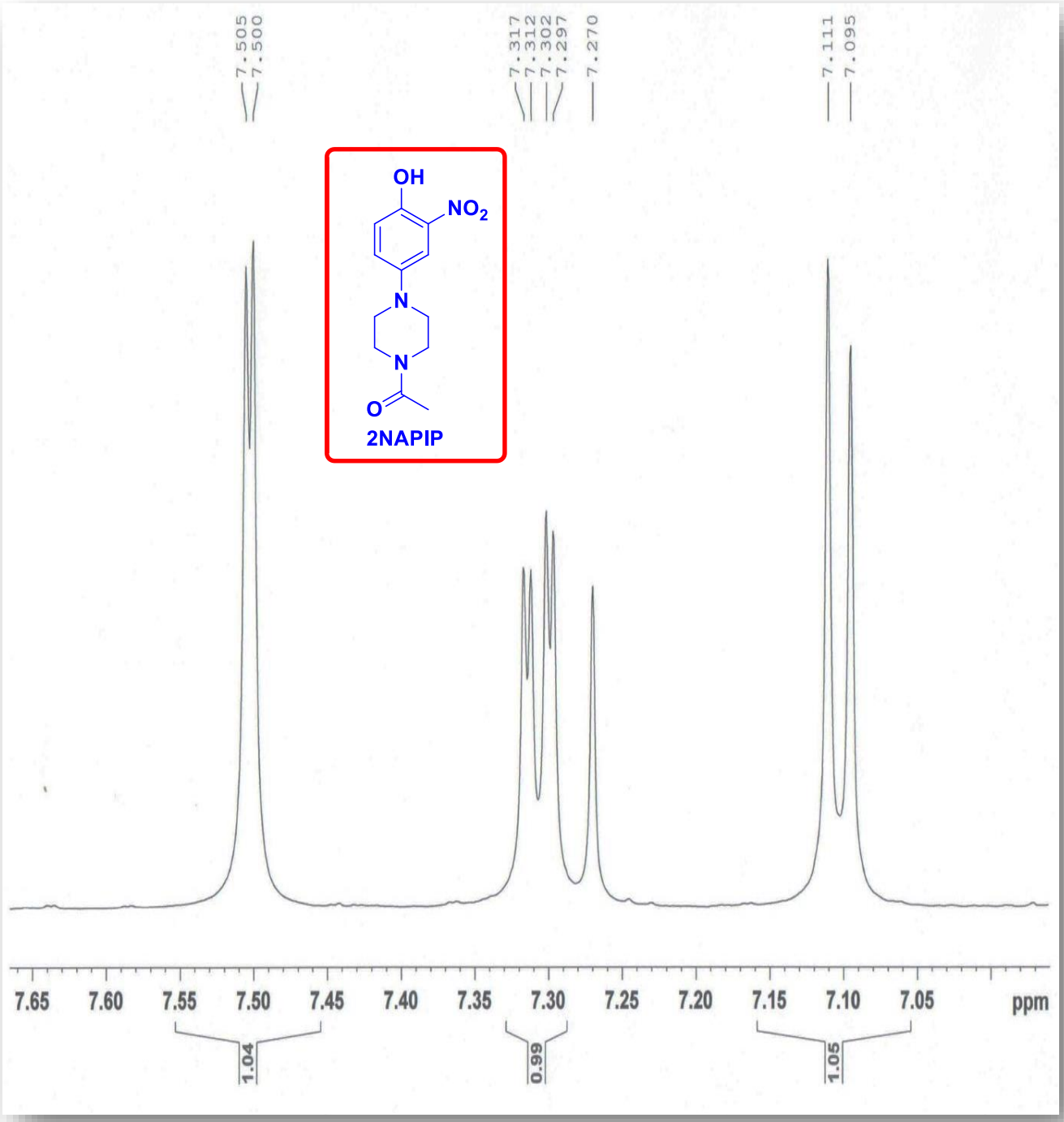

^{13}C NMR spectrum of 2NAPIP

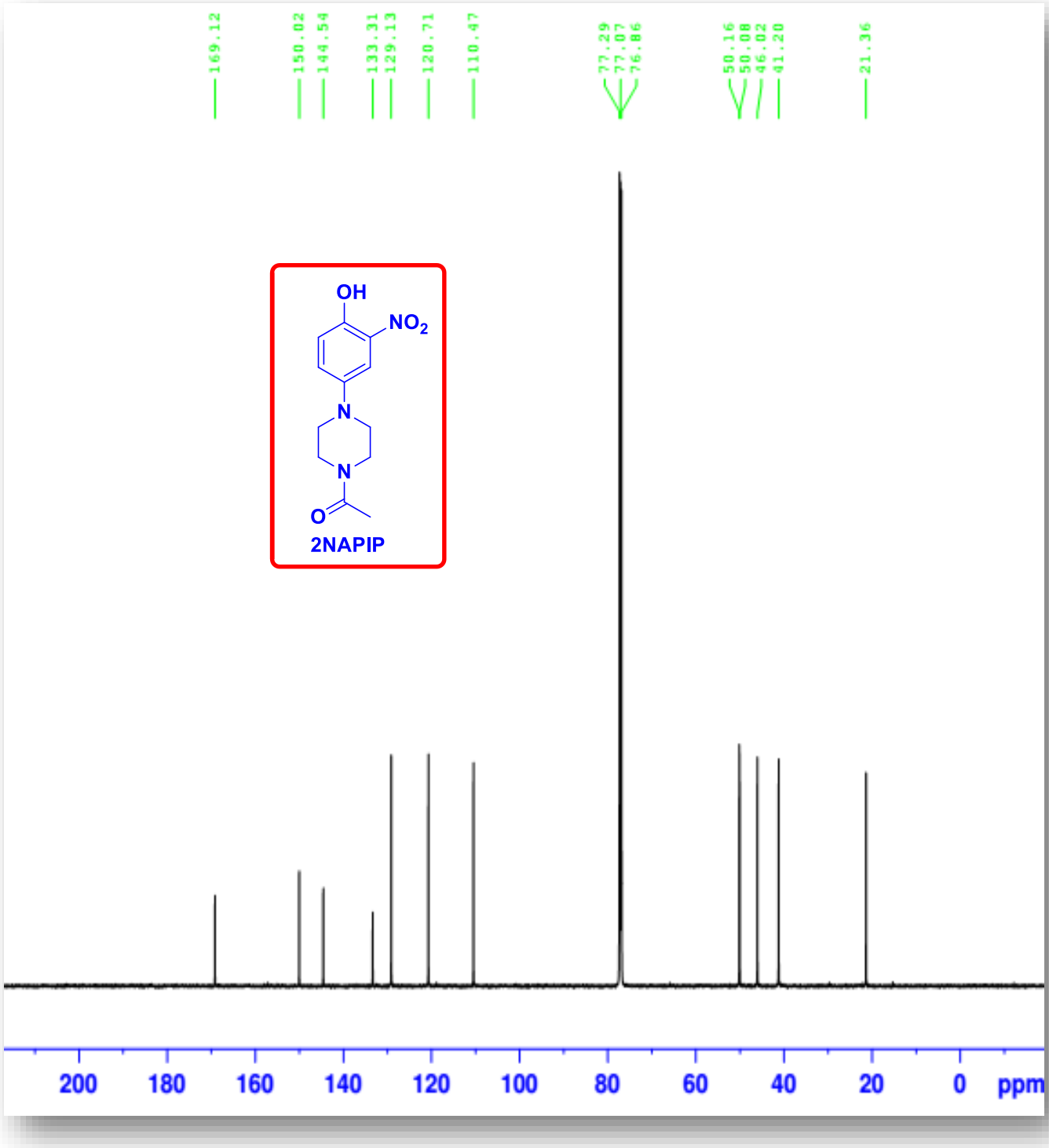

Expanded ^{13}C NMR spectrum of 2NAPIP

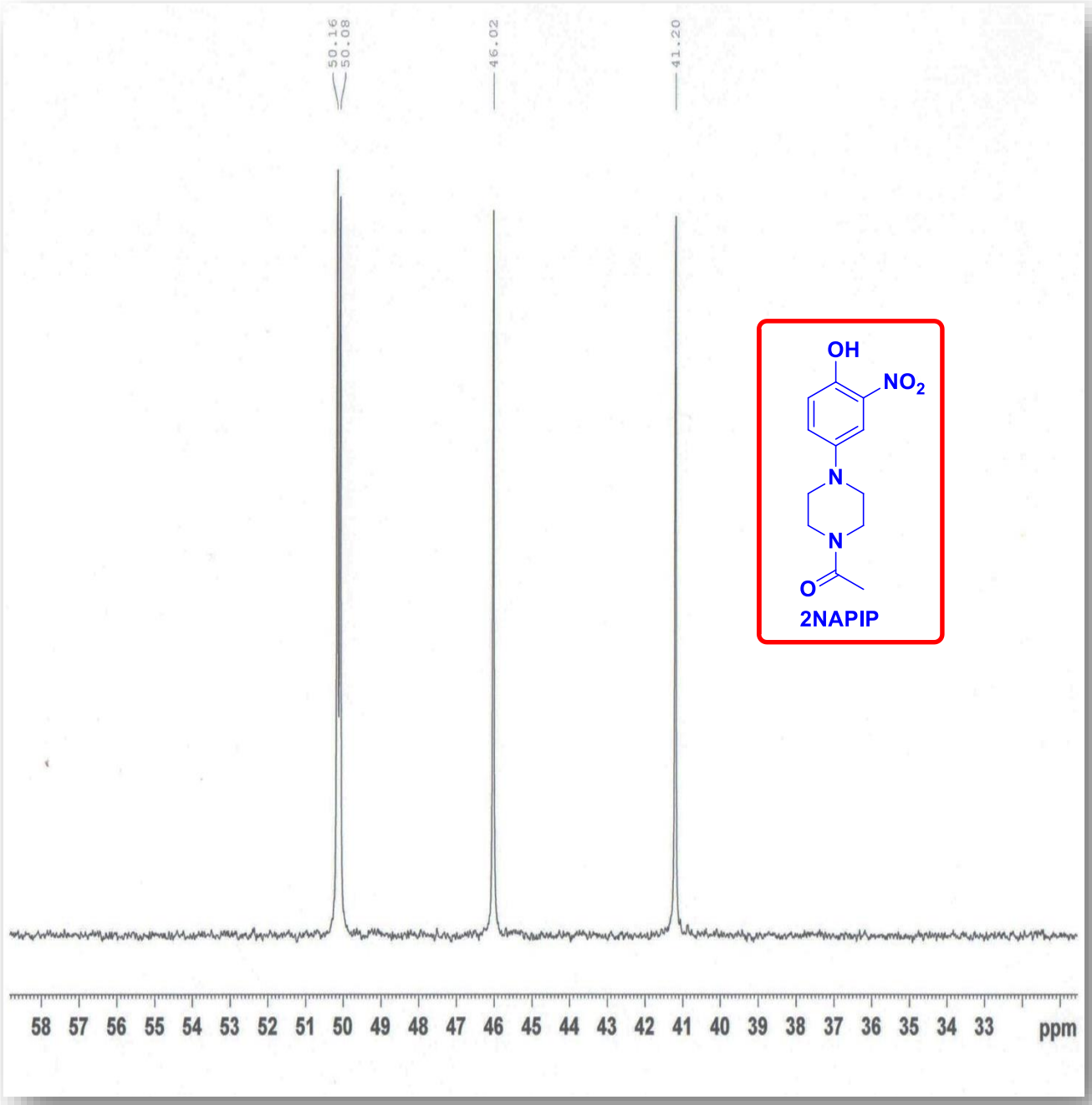

Cyclic voltammograms of APIP and 2NAPIP

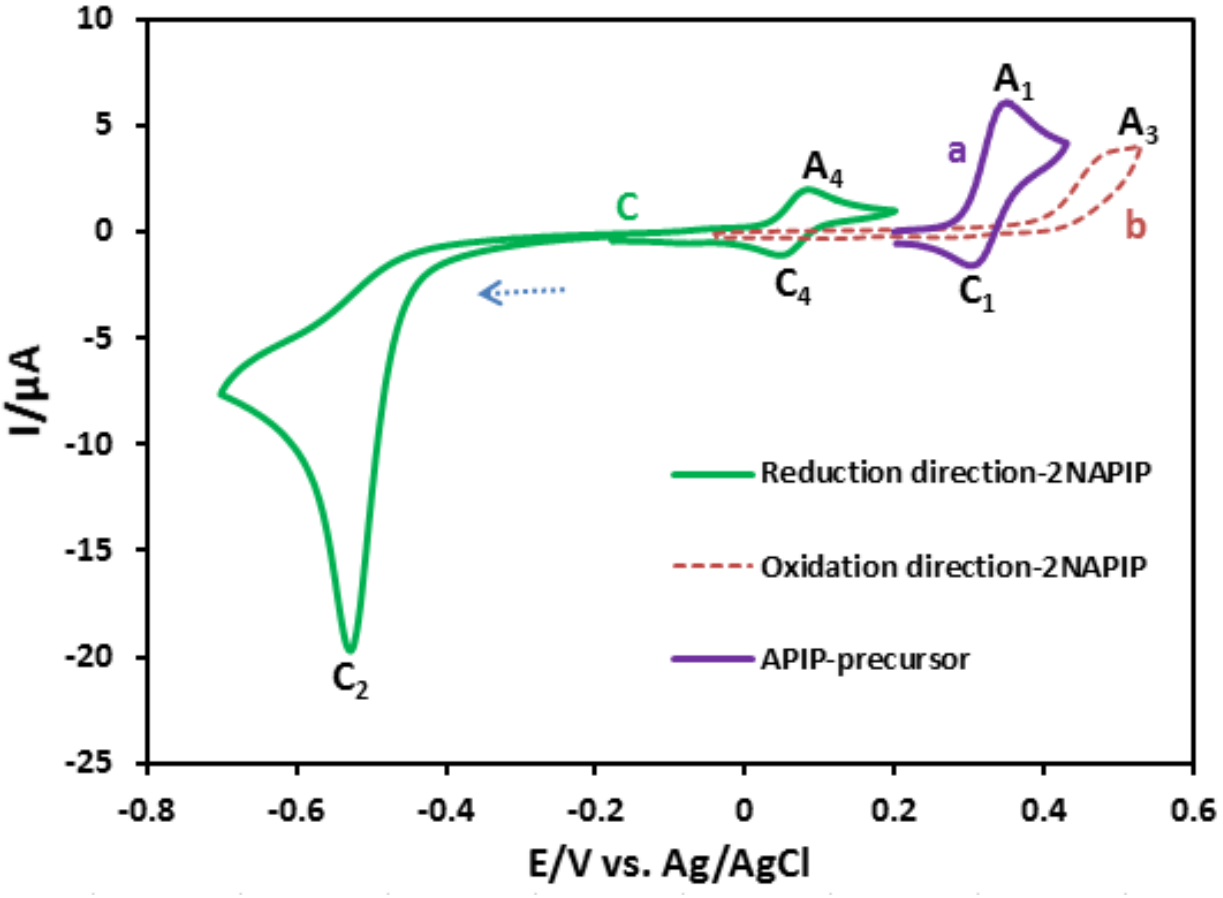

Fig. S7. (a) Cyclic voltammogram of **APIP**. (b) Cyclic voltammogram of **2NAPIP** starting from anodic direction. (c) Cyclic voltammogram of **2NAPIP** starting from cathodic direction. At glassy carbon electrode, in acetate buffer solution (*c* = 0.2 M, pH = 5.0). Concentration: 0.25 mM. Scan rate: 25 mV s^{-1}. Temperature =25 ± 1 ^{o}C

Calculated natural charge using BP86/Def2-TZVPP level of theory for PBQ and OBQ.

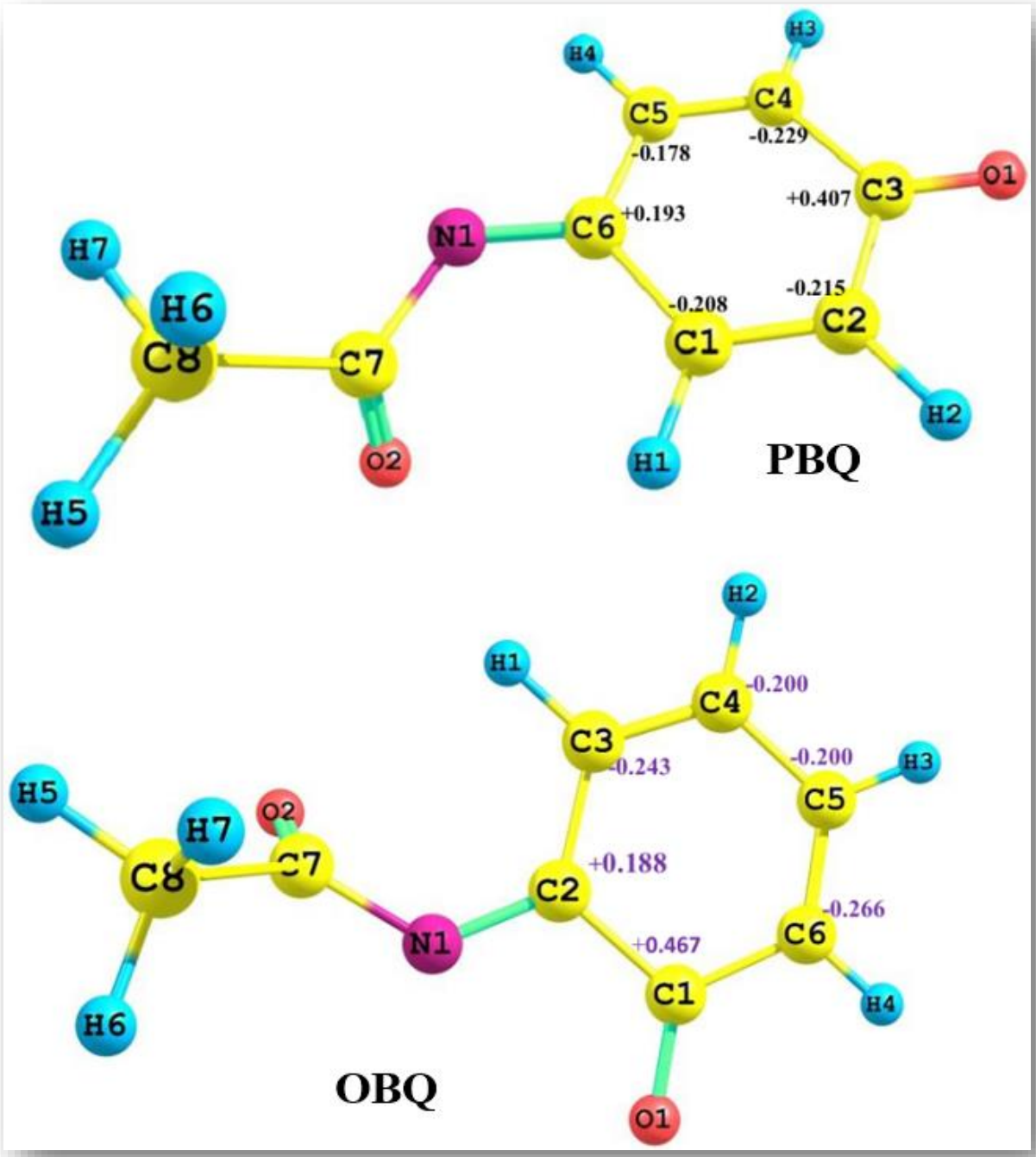

The chemical structures of the possible nitrated compounds

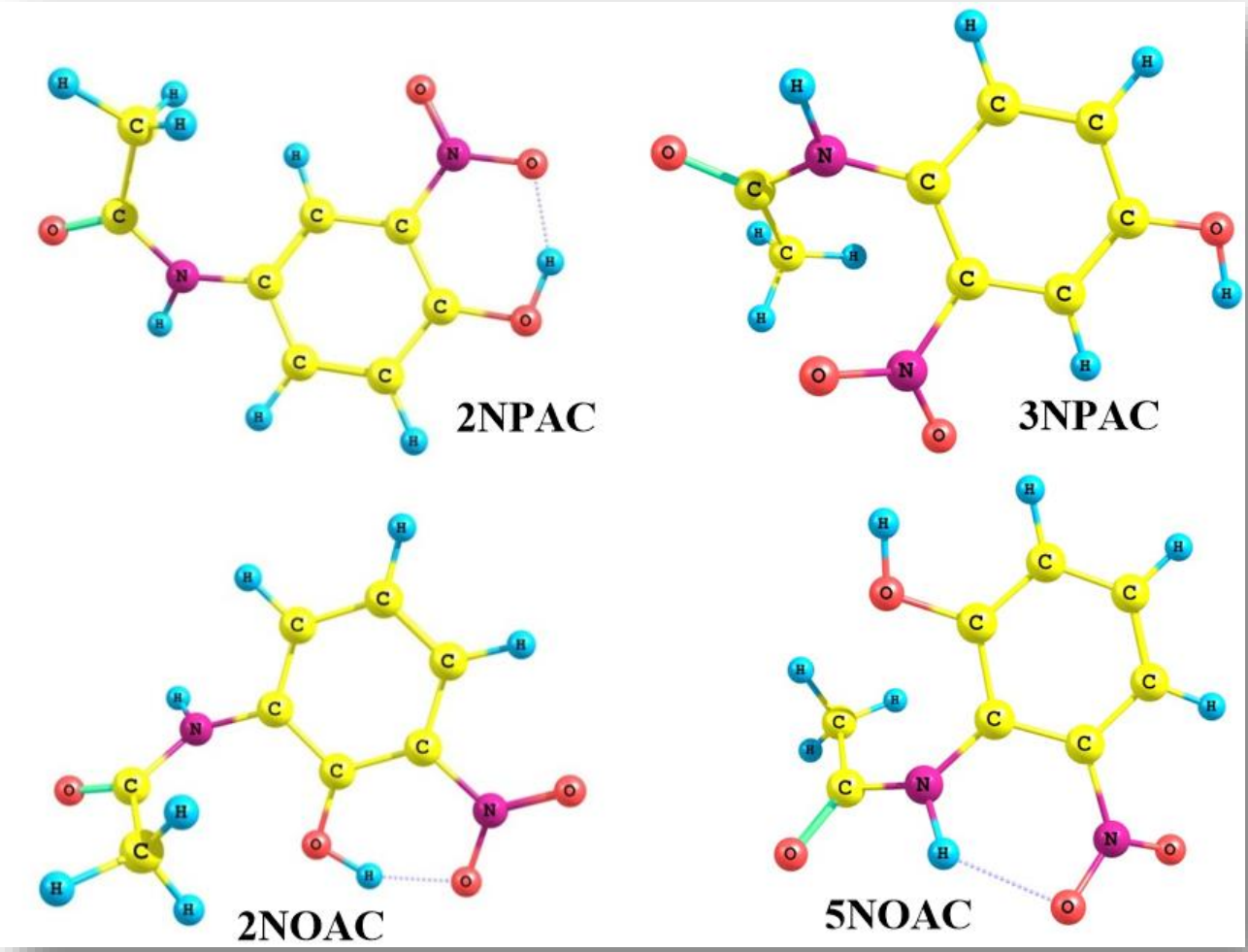

Calculated LUMO for 2NPAC, 3NPAC, 2NOAC and 5NOAC at level of BP86/Def2-TZVPP

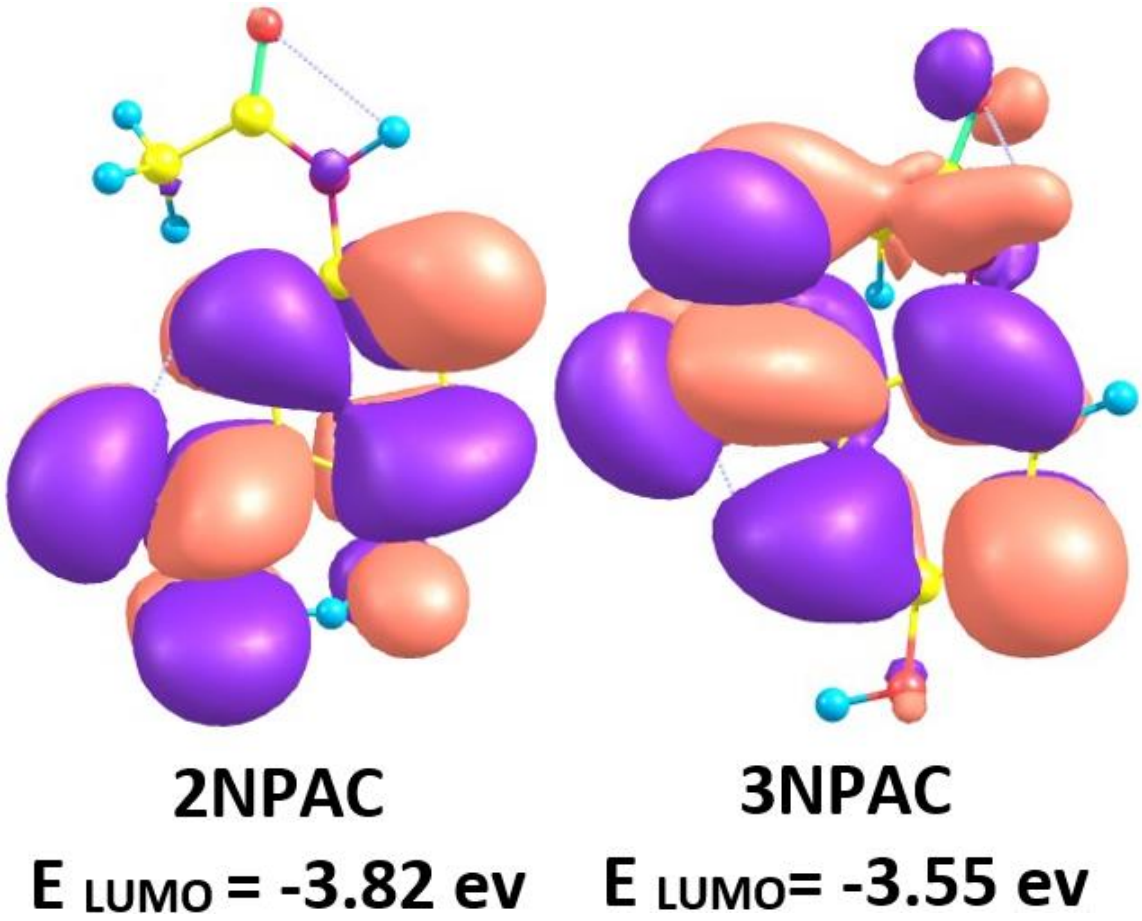

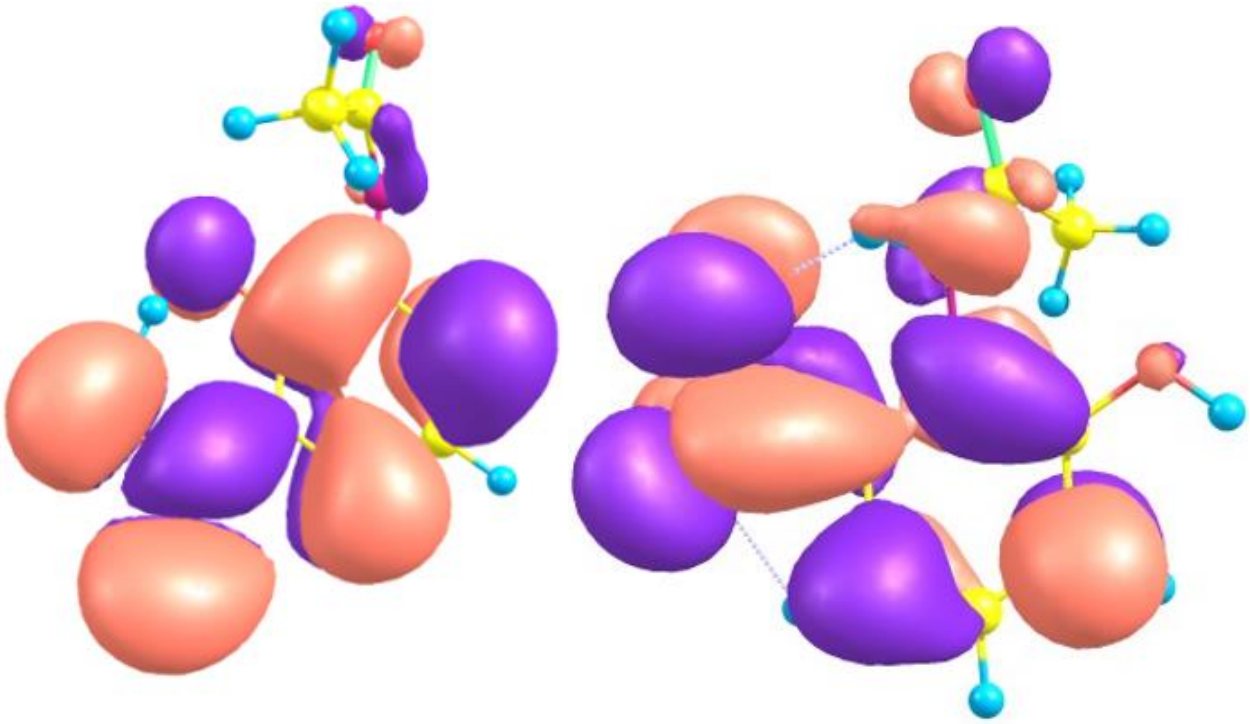

2NOAC

E LUMO = -3.93 ev

5NOAC

E LUMO= -3.54 ev

The molecular orbital analysis of latter compounds showed that the LUMO orbitals for both **2NPAC** and **2NOAC** which are more stable thermodynamically compounds are also more stable than corresponding **3NPAC** and **5NOAC.**

The LUMO coefficient of PBQ, OBQ and $APIP_{ox}$

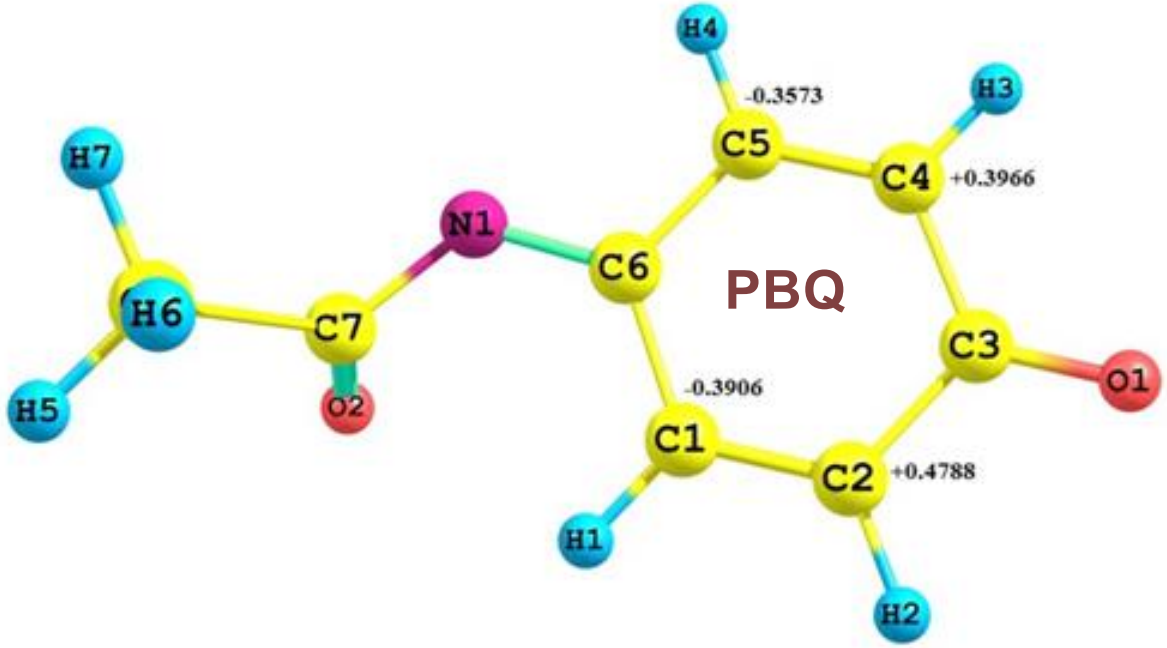

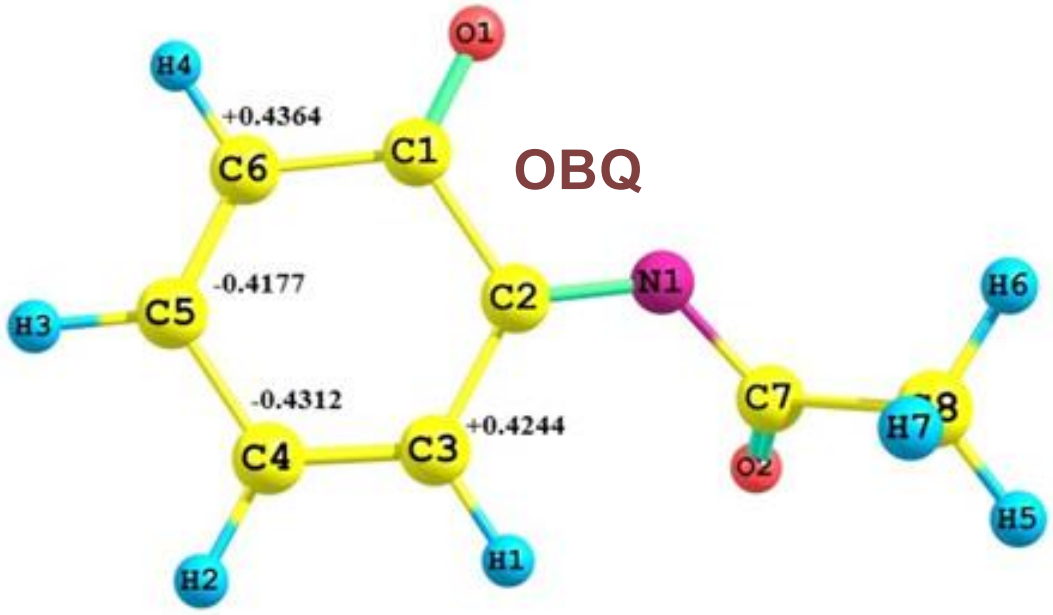

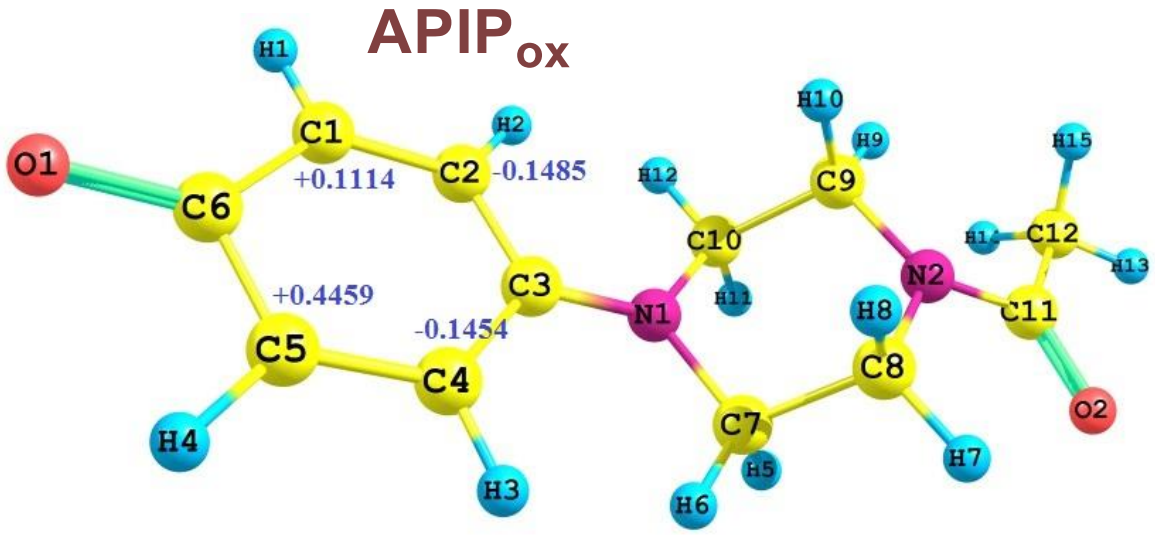

The calculations of LUMO coefficient of **PBQ**, **OBQ** and **APIP$_{ox}$** show that the LUMO coefficient of the carbon in the ortho position to the carbonyl carbon is larger than other carbons, which implies that a nucleophilic attack at this carbon should be favored.

Electrochemical oxidation of NHPA

In opposite to simple hydroxylamine aromatic compounds, *N*-(4-hydroxy-3-(hydroxyamino)phenyl)acetamid (**NHPA**) have two possible pathways for the oxidation (Scheme I).

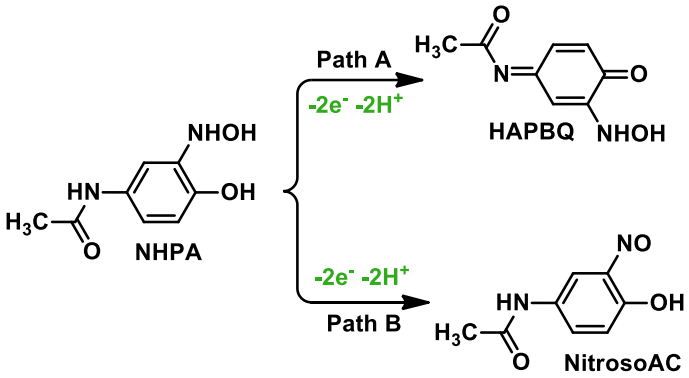

Scheme I. Possible pathways in electrochemical oxidation of **NHPA**.

However, since the electron releasing from the pink area is more feasible than hydroxylamine group.

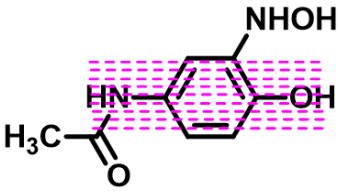

So, we think that electrochemical generation of **HAPBQ** (path A) is more probable than path B. On the other hand, we think that two forms (**HAPBQ** and **NitrosoAC**) can be converted to each other (Nematollahi-Salahifar rearrangement), as shown in Scheme II.

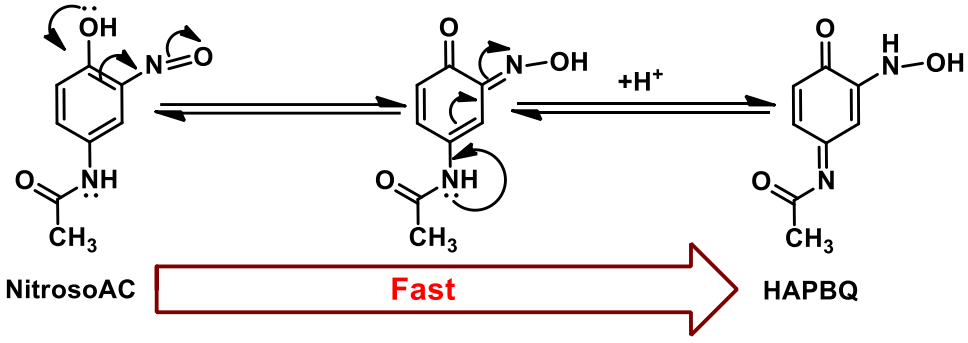

Scheme II. Interconversion between **nitrosoAC** and **HAPBQ** (Nematollahi-Salahifar rearrangement).

To study the interconversion between **nitrosoAC** and **HAPBQ** (Nematollahi-Salahifar rearrangement), in the first step, controlled-potential coulometry (CPC) of a solution containing **2NPAC** (0.25 mmol) was carried out in an acetate buffer solution (*c* = 0.2 M, pH = 5.0), at -0.58 V vs. Ag/AgCl. Fig. S8 displays the cyclic voltammograms of **2NPAC** during the CPC. The voltammograms show that in parallel to the disappearance of peak C_2, the current of anodic and cathodic peaks A_4/C4 increases. During the reaction **2NPAC** was converted to the corresponding hydroxylamine (**NHPA**) (Scheme III).

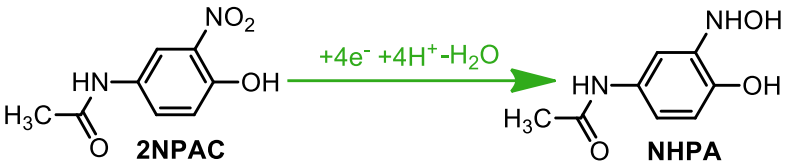

Scheme III. Electrochemical reduction of **2NPAC** to **NHPA**

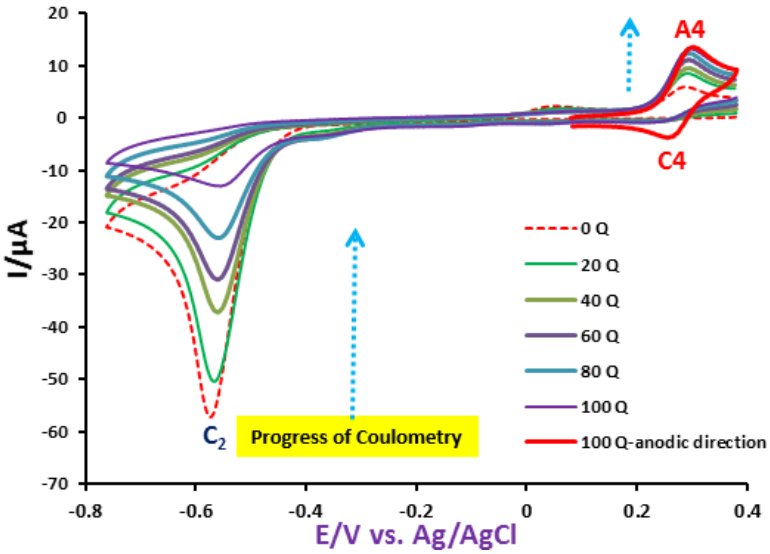

Fig. S8. Cyclic voltammograms of **2NPAC** (0.25 mmol) in an acetate buffer solution (*c* = 0.2 M, pH = 5.0) during the controlled potential coulometry at -0.58 V versus Ag/AgCl. Scan rate: 100 mV s^{-1}.

At the end of coulometry, the polarity of the electrode was reversed (at +0.25 V vs. Ag/AgCl). In these conditions, we consider two possibilities on the stability of **nitrosoAC**.

- The first possibility:

If the electrogenerated **nitrosoAC** is not stable and interconverts very fast to the **HAPBQ** as shown in Scheme II, then the azoxy derivative was not obtained and the theoretical charge consumption ($2e^-$) was obtained for the oxidation of **NHPA** (Scheme IV).

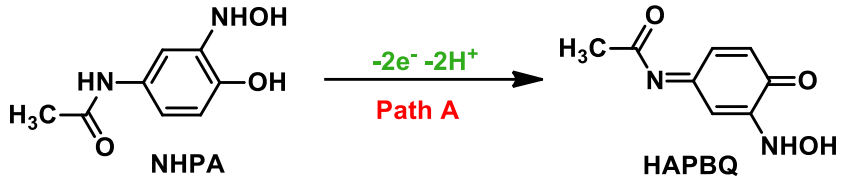

Scheme IV. Oxidative conversion of **NHPA** to **HAPBQ**.

- The second possibility:

If **nitrosoAC** is stable, it will react with the starting hydroxylamine and the azoxy compound was obtained as major product using less charge ($1e^-$) (for further data, see the valuable, published paper, B. A. Frontana-Uribe, C. Moinet, and L. Toupet, Eur. J. Org. Chem. 1999, 419) (Scheme V).

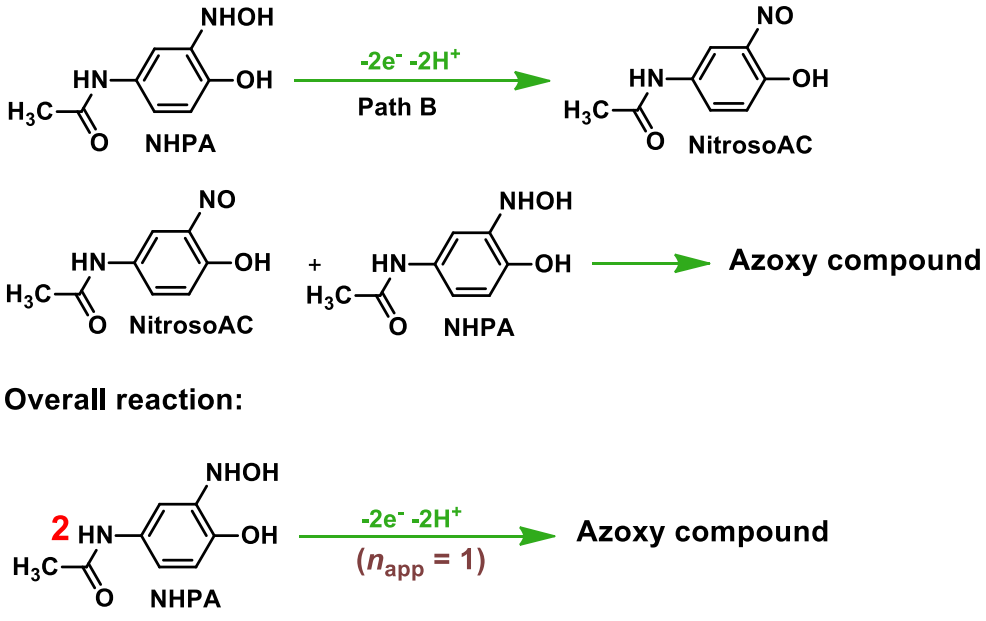

Scheme V. Electrochemical oxidation pathway of **NHPA**

Fig. S9 displays the cyclic voltammograms during the CPC at +0.25 V. The current of peak (A_4) (I_{pA4}) becomes about zero with the transfer of about **two electrons** per the starting molecule. This confirms the rapid tautomery of electrogenerated **nitrosoAC** to **HAPBQ.**

Finally, these data shows that during the electrochemical oxidation, **NHPA** directly (Scheme I, path a) or indirectly (generation of nitroso compound, and rapid tautomery of electrogenerated **nitrosoAC**) (Scheme II) was converted to **HAPBQ.**

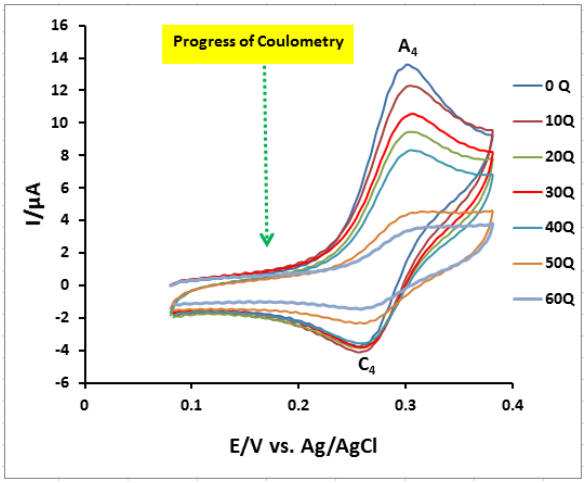

Fig. S9. Cyclic voltammograms of reduction product during controlled potential coulometry at +0.25 V versus Ag/AgCl. Scan rate: 100 mV s^{-1}.